SLC30A10 transporter in the digestive system regulates brain manganese under basal conditions while brain SLC30A10 protects against neurotoxicity

Received for publication, August 29, 2018, and in revised form, December 12, 2018 Published, Papers in Press, December 17, 2018, DOI 10.1074/jbc.RA118.005628

Cherish A. Taylor[‡1], **Steven Hutchens**[‡1], **Chunyi Liu**[‡], **Thomas Jursa**[§], **William Shawlot**[¶], **Michael Aschner**[‖], **Donald R. Smith**[§], **and Somshuvra Mukhopadhyay**[‡2]

From the [‡]*Division of Pharmacology and Toxicology, College of Pharmacy, Institute for Cellular and Molecular Biology, and Institute for Neuroscience and the* [¶]*Mouse Genetic Engineering Facility, University of Texas, Austin, Texas 78712, the* [§]*Department of Microbiology and Environmental Toxicology, University of California, Santa Cruz, California 95064, and the* [‖]*Department of Molecular Pharmacology, Albert Einstein College of Medicine, Bronx, New York 10461*

Edited by Paul E. Fraser

The essential metal manganese becomes neurotoxic at elevated levels. Yet, the mechanisms by which brain manganese homeostasis is regulated are unclear. Loss-of-function mutations in SLC30A10, a cell surface–localized manganese efflux transporter in the brain and liver, induce familial manganese neurotoxicity. To elucidate the role of SLC30A10 in regulating brain manganese, we compared the phenotypes of whole-body and tissue-specific *Slc30a10* knockout mice. Surprisingly, unlike whole-body knockouts, brain manganese levels were unaltered in pan-neuronal/glial *Slc30a10* knockouts under basal physiological conditions. Further, although transport into bile is a major route of manganese excretion, manganese levels in the brain, blood, and liver of liver-specific *Slc30a10* knockouts were only minimally elevated, suggesting that another organ compensated for loss-of-function in the liver. Additional assays revealed that SLC30A10 was also expressed in the gastrointestinal tract. In differentiated enterocytes, SLC30A10 localized to the apical/luminal domain and transported intracellular manganese to the lumen. Importantly, endoderm-specific knockouts, lacking SLC30A10 in the liver and gastrointestinal tract, had markedly elevated manganese levels in the brain, blood, and liver. Thus, under basal physiological conditions, brain manganese is regulated by activity of SLC30A10 in the liver and gastrointestinal tract, and not the brain or just the liver. Notably, however, brain manganese levels of endoderm-specific knockouts were lower than whole-body knockouts, and only whole-body knockouts exhibited manganese-induced neurobehavioral defects. Moreover, after elevated exposure, pan-neuronal/glial knockouts had higher manganese levels in the basal ganglia and thalamus than controls. Therefore, when manganese levels increase, activity of SLC30A10 in the brain protects against neurotoxicity.

This work was supported by NIEHS, National Institutes of Health, Grants R01-ES024812 and R01-ES024812S1 (to S. M.). The authors declare that they have no conflicts of interest with the contents of this article. The content is solely the responsibility of the authors and does not necessarily represent the official views of the National Institutes of Health.
This article contains Figs. S1–S10.
[1] Both authors contributed equally to this work.
[2] To whom correspondence should be addressed: Division of Pharmacology and Toxicology, University of Texas, 3.510E BME, 107 W. Dean Keeton St., Austin, TX 78712. E-mail: som@austin.utexas.edu.

Manganese is essential, but elevated levels are neurotoxic (1). Toxicity may occur due to exposure from occupational or environmental sources (2–5). Additionally, manganese is primarily excreted by the liver via transport into bile (6–10). Patients with hepatic dysfunction fail to excrete manganese and develop neurotoxicity in the absence of elevated exposure (11). The primary manifestation of toxicity in adults is a parkinsonian-like movement disorder (2, 3). Exposure during childhood and adolescence is associated with emotional, cognitive, and intellectual deficits (12). Despite the clinical relevance, mechanisms by which manganese homeostasis is regulated at the whole-animal level in general, and in the brain in particular, remain unclear. This has hindered therapeutic progress.

In 2012, homozygous loss-of-function mutations in *SLC30A10* were reported to cause the first inherited disorder of manganese metabolism that induced neurotoxicity in humans (13–17). Manganese levels were elevated in the brain, liver, and blood of patients, but there was no history of exposure to elevated manganese (14, 16). Autopsy of one patient revealed neuronal loss in the globus pallidus (13), which also characterizes manganese toxicity secondary to occupational overexposure (2, 3). Further, SNPs in SLC30A10 were associated with increased blood manganese and altered neurological function in the general population (18). We demonstrated that SLC30A10 functioned as a cell surface–localized manganese efflux transporter that reduced cellular manganese levels and protected against toxicity (19–21). Moreover, we generated whole-body *Slc30a10* knockout mice and reported that these animals had markedly high manganese levels in the brain, liver, blood, and thyroid (22, 23). Overall, available data identify SLC30A10 to be a critical regulator of manganese homeostasis and detoxification.

Despite the above studies, the fundamental question of how manganese homeostasis in the brain is regulated is unclear. In humans and mice, SLC30A10 was detected in the brain, including in basal ganglia neurons (13, 14, 22, 23). Thus, one possibility is that activity of SLC30A10 in the central nervous system may regulate brain manganese homeostasis. Interestingly, however, SLC30A10 was also detected in the liver (13, 14, 22, 23). In differentiated HepG2 cells, SLC30A10 localized to the canalicular/apical domain (23). Moreover, as described earlier, liver manganese levels were substantially elevated in whole-body

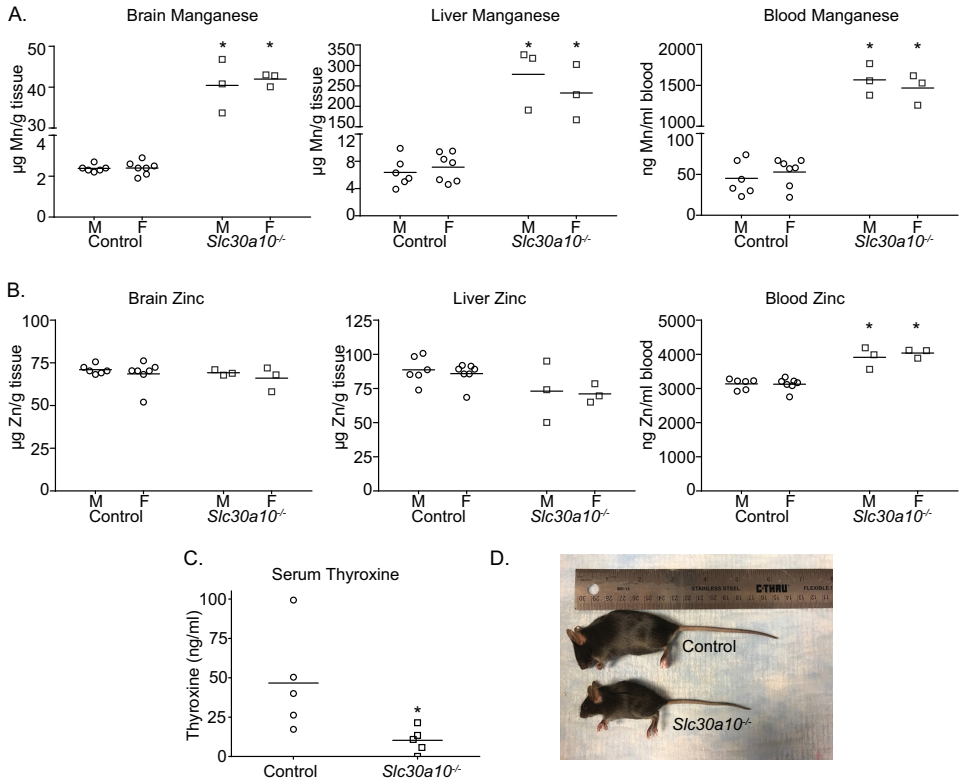

Figure 1. Whole-body *Slc30a10* knockout mice develop severe manganese toxicity. *A* and *B*, tissue metal levels were measured in 4-week old littermate control or whole-body *Slc30a10* knockout ($Slc30a10^{-/-}$) mice. $n = 6$ male and 7 female controls and 3 male and 3 female knockouts. *Line*, mean. *, $p < 0.05$ by two-way ANOVA and Sidak's post hoc test for differences between genotypes compared in a sex-specific manner. *C*, serum thyroxine levels were measured in 6-week-old male littermate controls or knockouts. Only males were used because our prior assays revealed that hypothyroidism was more severe in males (22). $n = 5$/group. *Line*, mean. *, $p < 0.05$ by *t* test. *D*, photograph of a 6-week-old male knockout and its male littermate control.

Slc30a10 knockout mice (22, 23). These results indicate that activity of SLC30A10 in the liver is crucial for hepatic manganese excretion (23). Thus, a second possibility is that tissue manganese levels, including in the brain, may be controlled by the activity of SLC30A10 in the liver. Determining the mechanisms by which the function of SLC30A10 in different organs regulates brain manganese is an essential step in elucidating the pathobiology of manganese neurotoxicity.

To address this issue, we compared the phenotypes of tissue-specific and whole-body *Slc30a10* knockout mice. We report the surprising finding that, under basal physiological conditions, activity of SLC30A10 in the entire digestive system, and not the brain or just the liver, regulates brain manganese. Expression of SLC30A10 in the brain becomes important when tissue manganese levels increase; under these conditions, activity of SLC30A10 in the brain reduces manganese levels and protects against neurotoxicity. Our findings identify the digestive system, including extrahepatic components, as a critical mediator in the biology of manganese neurotoxicity at the whole-organism level. Additionally, these results imply that there are previously unappreciated complexities in the homeostatic control of manganese in the brain under basal and elevated exposure conditions.

Results

Brain manganese levels are markedly elevated in whole-body Slc30a10 knockouts

As a positive control for the current study, we recapitulated the previously described phenotype of whole-body *Slc30a10* knockout mice (referred to as $Slc30a10^{-/-}$ mice here) in a new cohort analyzed contemporaneously with tissue-specific knockouts. Consistent with prior results (22, 23), compared with littermate controls, the new cohort of $Slc30a10^{-/-}$ animals exhibited ~20–40-fold elevations in brain, liver, and blood manganese (Fig. 1*A*). There were no changes in brain or liver zinc levels (Fig. 1*B*). A mild elevation in blood zinc was observed (Fig. 1*B*). Prior studies in cell culture, *Caenorhabditis elegans*, $Slc30a10^{-/-}$ mice, and human patients indicate that SLC30A10 transports manganese, but not zinc (14, 16, 17, 19–26), implying that the changes in blood zinc observed in the current cohort were likely secondary to those in manganese. Additionally, we previously demonstrated that $Slc30a10^{-/-}$ mice were smaller in size than littermate controls and developed hypothyroidism due to a block in intrathyroid thyroxine production induced by elevated thyroid manganese levels (22, 23). Consistent with this, $Slc30a10^{-/-}$ mice in the current cohort were also hypothyroid and substantially smaller in size than littermates (Fig. 1, *C* and *D*).

Brain manganese levels of pan-neuronal/glial Slc30a10 knockouts are comparable with littermate controls

In the central nervous system, SLC30A10 is expressed in neurons (13, 14), but thus far, expression in nonneuronal cells has not been reported. To deplete SLC30A10 in neurons, we crossed homozygous floxed *Slc30a10* mice ($Slc30a10^{fl/fl}$) with the widely used nestin (Nes)-*Cre* strain, which induces recombination in neuronal and glial (astrocytes and oligodendro-

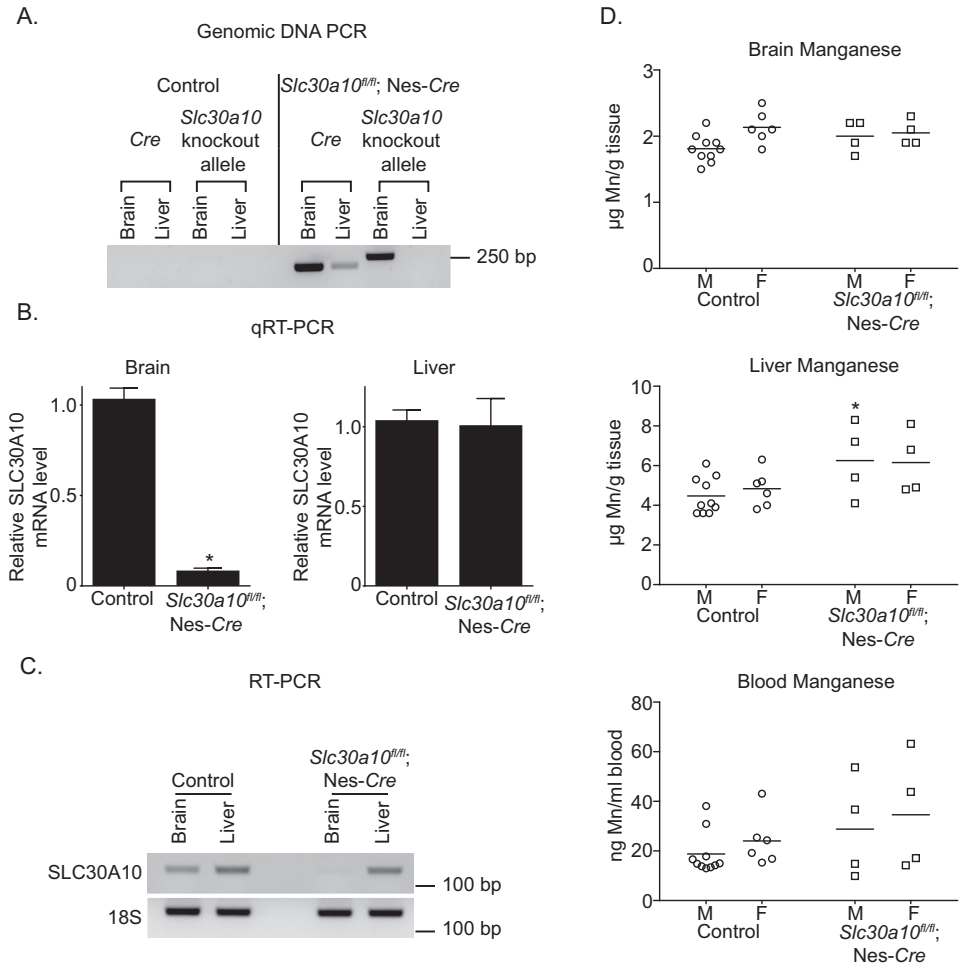

Figure 2. Brain manganese levels are unaltered in pan-neuronal/glial *Slc30a10* knockouts. *A*, PCR assays were performed to detect the recombined *Slc30a10* allele and the *Cre* transgene using genomic DNA samples isolated from the liver or brain of pan-neuronal/glial knockouts or littermate controls. *B*, QRT-PCR analyses were performed to assay for SLC30A10 mRNA levels in pan-neuronal/glial knockouts or littermate controls. $n \geq 3$/group. Results shown are mean ± S.E. (*error bars*). *, $p < 0.05$ by *t* test. *C*, RT-PCR analyses were performed to detect SLC30A10 and 18S mRNA in pan-neuronal/glial knockouts or littermate controls. *D*, tissue manganese levels were measured in 3-month-old pan-neuronal/glial knockouts or littermate controls. $n = 10$ male and 6 female controls and 4 male and 4 female knockouts. *Line*, mean. *, $p < 0.05$ by two-way ANOVA and Sidak's post hoc test for differences between genotypes compared in a sex-specific manner.

cytes) precursors (27, 28). We refer to these knockouts as pan-neuronal/glial knockouts (also denoted as *Slc30a10*$^{fl/fl}$;Nes-*Cre* mice). Glia are critical regulators of neural function, and use of the Nes-*Cre* strain ensured that results would not be confounded by as yet undetected expression of SLC30A10 in glia.

We genotyped tissue-specific knockouts used in this study by performing PCR from genomic DNA isolated from ear punches or tail snips to detect the WT or floxed *Slc30a10* allele and the *Cre* transgene. For selected animals, we confirmed the genotype by performing two separate assays. First, we used PCR to ensure that the recombined (*i.e.* knockout) *Slc30a10* allele was detected only in genomic DNA extracted from the tissue targeted by the *Cre* transgene. Second, we assayed for SLC30A10 mRNA using RT-PCR and qRT-PCR.[3] Protein-based assays could not be performed because antibodies that specifically detect SLC30A10 protein in rodent tissue are not available. (We generated a custom antibody against the C terminus of the human protein, but this antibody appears to lose specificity when rodent tissue samples are used (22, 23); also see "Experimental procedures.")

In PCR assays, in the pan-neuronal/glial knockouts, the recombined *Slc30a10* allele was detected in the brain, but not the liver, whereas the *Cre* transgene was amplified from both organs (Fig. 2*A*). Importantly, the recombined allele was not detected in the brain or the liver of littermate controls (Fig. 2*A*). Moreover, compared with littermate controls, levels of SLC30A10 mRNA in the brain, but not in the liver, of the pan-neuronal/glial knockouts were substantially lower (Fig. 2, *B* and *C*). Thus, in *Slc30a10*$^{fl/fl}$;Nes-*Cre* mice, SLC30A10 was specifically depleted in the brain.

We anticipated that brain manganese levels of the *Slc30a10*$^{fl/fl}$;Nes-*Cre* mice would be greater than in littermate controls. Contrary to our expectation, brain manganese levels of the pan-neuronal/glial knockouts were comparable with those of littermate controls (Fig. 2*D*). Analyses of other organs identified a mild elevation in liver manganese (Fig. 2*D*); although statistically significant, the biological relevance of this small increase is unclear. Blood manganese levels of

[3] The abbreviations used are: qRT-PCR, quantitative RT-PCR; ANOVA, analysis of variance.

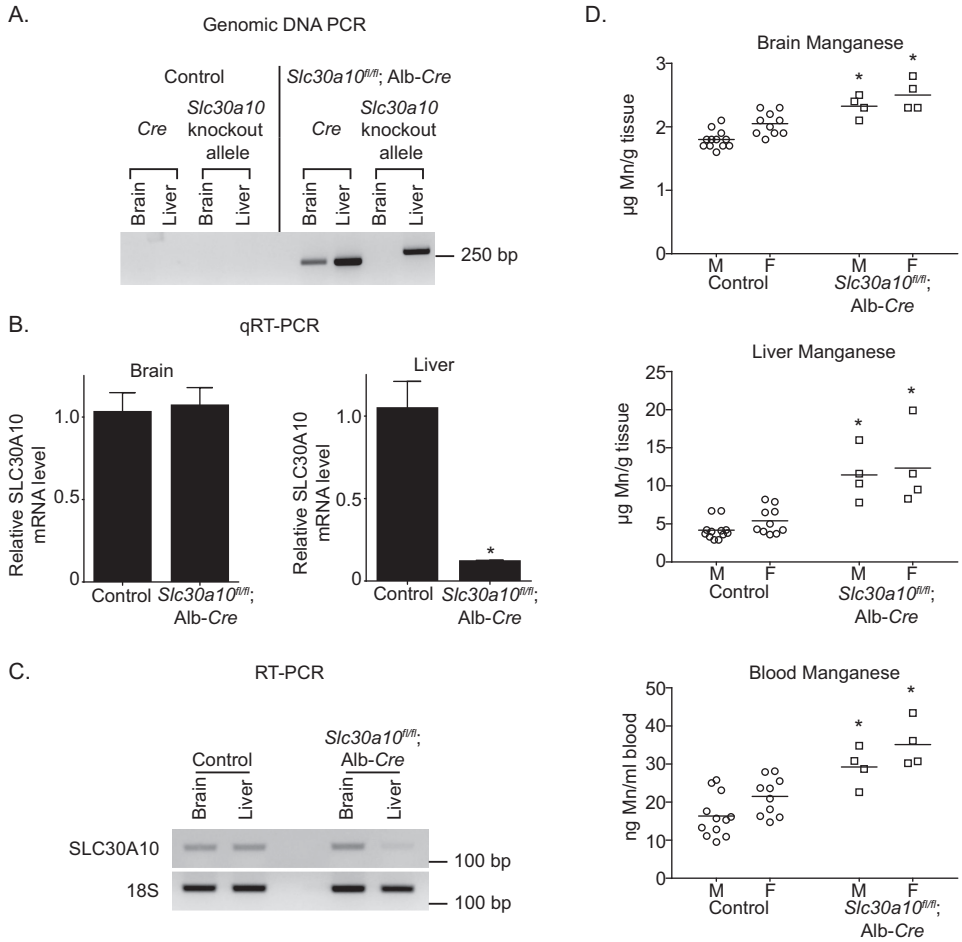

Figure 3. Tissue manganese levels are only minimally elevated in liver-specific *Slc30a10* knockouts. *A*, PCR assays were performed to detect the recombined *Slc30a10* allele and the *Cre* transgene. *B*, levels of SLC30A10 mRNA were quantified using qRT-PCR. $n = 3$/group. Results shown are mean ± S.E. (*error bars*). *, $p < 0.05$ by *t* test. *C*, RT-PCR assays were used to detect SLC30A10 and 18S mRNA. *D*, tissue manganese levels were measured in 3-month-old knockouts or littermate controls. $n = 12$ male and 10 female controls and 4 male and 4 female knockouts. *Line*, mean. *, $p < 0.05$ by two-way ANOVA and Sidak's post hoc test for differences between genotypes compared in a sex-specific manner.

Slc30a10$^{fl/fl}$;Nes-*Cre* mice were comparable with controls (Fig. 2*D*). We verified that levels of other metals (zinc, iron, and copper) in brain, liver, and blood were not altered (Fig. S1, *A–C*). Thus, expression of *Slc30a10* in the brain is not required to regulate brain manganese under basal physiological conditions.

Brain manganese levels of liver-specific Slc30a10 knockouts are only minimally increased

We then generated liver-specific *Slc30a10* knockouts by crossing *Slc30a10*$^{fl/fl}$ mice with albumin (Alb)-*Cre* mice (29), anticipating that these animals would exhibit marked elevations in tissue manganese levels due to decreased manganese excretion (the liver-specific knockouts are denoted as *Slc30a10*$^{fl/fl}$;Alb-*Cre*). As expected, in the liver-specific knockouts, the recombined *Slc30a10* allele was detected in the liver, but not the brain, and SLC30A10 mRNA was depleted in the liver, but not the brain (Fig. 3, *A–C*). Surprisingly, compared with littermate controls, brain, liver, and blood manganese levels of *Slc30a10*$^{fl/fl}$;Alb-*Cre* mice were only modestly elevated by ~1.5–2.5-fold (Fig. 3*D*). The change in manganese was specific because levels of zinc, iron, and copper did not increase (Fig. S2, *A–C*). Thus, loss-of-function of *Slc30a10* in the liver has only a modest impact on manganese levels in the liver and in extrahepatic organs, including the brain.

SLC30A10 mediates manganese efflux from the apical/luminal domain of polarized enterocytes

Although hepatic excretion is the main route of manganese elimination (6–10), prior studies indicate that a pool of manganese may also be excreted by parts of the gastrointestinal tract (*e.g.* intestines) and that the role of the gastrointestinal tract gains prominence when hepatic excretion is compromised (6, 8). RT-PCR analyses revealed that, in the gastrointestinal tract, SLC30A10 was expressed in the intestines as well as in the stomach and esophagus (Fig. 4*A*). This observation raised the hypothesis that, in the liver-specific knockouts, activity of SLC30A10 in the intestines (and possibly other parts of the gastrointestinal tract that express SLC30A10) compensated for loss-of-function in the liver.

To test this hypothesis, we first performed experiments in culture using CaCo2 cells. These cells are a human intestinal epithelial cancer cell line that, upon differentiation, assume characteristics of enterocytes (30). Intestinal enterocytes are polarized cells with an apical/luminal domain that transports substances to or from the intestinal lumen and a basolateral

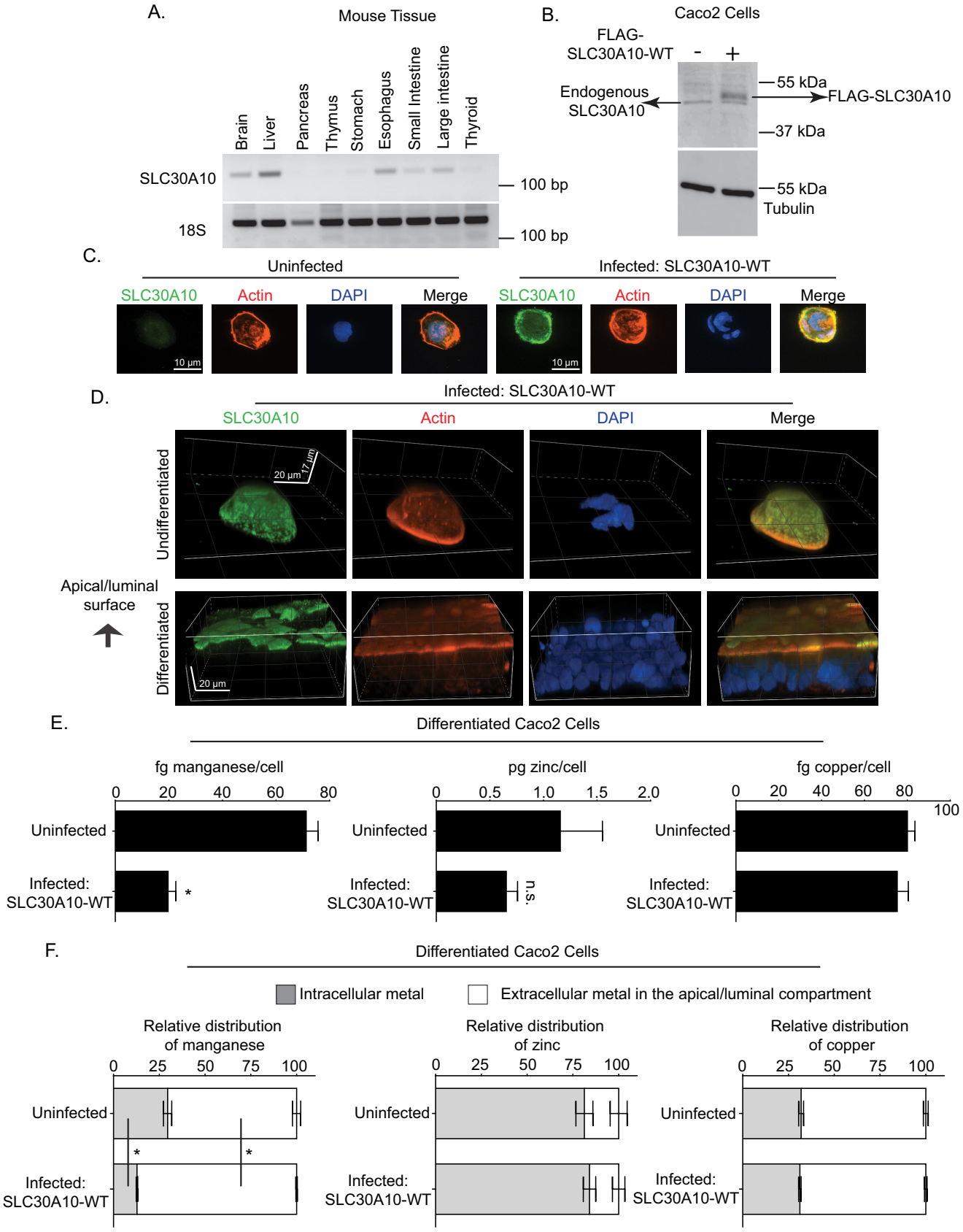

domain that interfaces with the capillary network (30). To mediate manganese excretion, SLC30A10 must localize to the apical/luminal domain of differentiated enterocytes (localization to the basolateral domain would lead to the absorption of manganese from enterocytes into blood). In undifferentiated CaCo2 cells, expression of endogenous SLC30A10, detected using our custom SLC30A10 antibody, was low (Fig. 4, *B* and *C*). Therefore, we generated a stable CaCo2 subline in which FLAG-tagged human SLC30A10 WT (*i.e.* full-length) was overexpressed using lentivirus (Fig. 4, *B* and *C*). Notably, immunofluorescence analyses revealed that, in undifferentiated cells that overexpressed SLC30A10, the SLC30A10 protein localized to the cell surface (Fig. 4*C*). We then used this subline to compare the localization of SLC30A10 with or without differentiation. In undifferentiated cells, SLC30A10 was detected on all aspects of the cell surface in three dimensions (Fig. 4*D*). Prior studies show that F-actin localizes to the apical/luminal domain of differentiated CaCo2 cells (30). Consistent with this, in our experiments, unlike in undifferentiated cells, F-actin predominantly localized to the apical/luminal domain of differentiated cells (Fig. 4*D*), indicating that the differentiation was successful. Importantly, after differentiation, SLC30A10 also localized to the apical/luminal domain (Fig. 4*D*).

Next, we sought to obtain direct functional evidence of the manganese transport activity of SLC30A10 from the apical/luminal domain. For this, we first compared intracellular metal levels in differentiated CaCo2 cells that did or did not overexpress SLC30A10 after treatment with 12.5 μM manganese for 16 h. Manganese was added to the basal compartment of the culture dish (media bathing the basal and apical compartments are distinct; see Fig. S3*A* and "Experimental procedures"). We verified that the manganese treatment did not alter cell viability or induce toxicity. Importantly, levels of intracellular manganese, but not zinc or copper, were lower in the overexpressing cells (Fig. 4*E*). To validate that the reduction in intracellular manganese was due to an increase in manganese efflux from the apical/luminal domain, we performed a pulse-chase experiment in which we treated cells with 12.5 μM manganese for 16 h and then chased the cells in manganese-free media for 1 h (see "Experimental procedures"). Analyses of metal levels after the chase revealed that, in cells overexpressing SLC30A10, there was an increase in the amount of manganese released into the media of the apical/luminal compartment and a decrease in the amount of manganese retained within cells (Fig. 4*F* and Fig. S3*B*). Levels of zinc or copper in both compartments were comparable between cells that did or did not overexpress SLC30A10 (Fig. 4*F*). Thus, SLC30A10 has the capability to mediate efflux of manganese from the apical/luminal domain of differentiated enterocytes.

Endoderm-specific knockouts of Slc30a10 exhibit substantial elevations in tissue manganese levels and are hypothyroid

To determine whether activity of SLC30A10 in the liver and intestines (and possibly stomach and esophagus, which also express SLC30A10) cooperatively regulate tissue manganese levels in mice, we took advantage of the fact that the liver, epithelial lining of the gastrointestinal tract, gallbladder, and pancreas are all derived from the endoderm (31). Use of the Foxa3-*Cre* strain, which induces recombination in all endoderm-derived tissues during early embryonic development (32, 33), provided a straightforward means to deplete SLC30A10 in the entire digestive system (the endoderm-specific knockouts are denoted as *Slc30a10*$^{fl/fl}$;Foxa3-*Cre*). Note that the Foxa3-*Cre* strain has been extensively used as a tool to induce recombination in the digestive system (32–34), and clear expression of SLC30A10 mRNA was not detectable in the other endoderm-derived tissues tested (thymus and thyroid) (23, 31) (Fig. 4*A*), implying that loss of SLC30A10 function in these organs would not impact manganese homeostasis (*Slc30a10*$^{-/-}$ mice develop hypothyroidism, but *Slc30a10* itself is not expressed in the thyroid; the hypothyroidism occurs due to the accumulation of manganese in the thyroid secondary to increased body levels (23)). Also note that we did not generate an intestine-specific *Slc30a10* knockout for this study, using the Villin-*Cre* strain (35), because expression of SLC30A10 in the liver (as well as esophagus and stomach) would not be depleted in the intestinal knockouts, and as described earlier, the liver plays a major role in manganese excretion (6–10).

In the endoderm-specific knockouts, the recombined *Slc30a10* allele was detected in the liver and intestines, but not the brain (Fig. 5*A*). Additionally, compared with littermate controls, levels of SLC30A10 mRNA in the liver and intestines, but not the brain, of the endoderm-specific knockouts were depleted (Fig. 5, *B* and *C*). Importantly, the phenotype of *Slc30a10*$^{fl/fl}$;Foxa3-*Cre* mice had striking similarities to the whole-body knockouts. Compared with littermate controls, the endoderm-specific knockouts were smaller in size, and by 6 weeks of age, body weights of the knockouts were ~50% lower than controls (Fig. 5, *D* and *E*). Knockouts died between 7 and 8 weeks of age. Metal measurements revealed that manganese levels in the brain, liver, blood, and thyroid of the knockouts were ~10–40-fold greater than littermate controls (Fig. 5*F*). By 6 weeks of age, serum thyroxine levels of the endoderm-specific knockouts were lower than controls (Fig. 5*G*), implying that

Figure 4. SLC30A10 localizes to, and mediates manganese efflux from, the apical/luminal domain of differentiated CaCo2 cells. *A*, RT-PCR was performed to detect SLC30A10 and 18S mRNA in tissue isolated from 4-week-old control male mice. *B*, immunoblot analyses were performed to detect SLC30A10, using the custom antibody against the C terminus of human SLC30A10, and tubulin, using a mAb, in undifferentiated CaCo2 cells that did or did not overexpress FLAG-tagged SLC30A10 WT. *C*, undifferentiated CaCo2 cells that did or did not overexpress SLC30A10 WT were imaged to detect SLC30A10, using the custom polyclonal antibody against the C terminus of SLC30A10; actin, using fluorescently labeled phalloidin; and nuclei, using 4′,6-diamidino-2-phenylindole (*DAPI*). *Scale bars*, 10 μm. *D*, CaCo2 cells that overexpressed SLC30A10 WT were either left undifferentiated or differentiated for 4 weeks as described under "Experimental procedures." Cells were then imaged to detect SLC30A10, actin, and nuclei as described above. Images are depicted in three dimensions. *Scale bars* in the *xy* and *z* dimensions are indicated in the panels. *E*, CaCo2 cells that did or did not overexpress SLC30A10 WT were differentiated for 4 weeks. After this, cells were treated with 12.5 μM manganese for 16 h. Manganese was added to the media in the basal compartment. Intracellular metal levels were then analyzed as described under "Experimental Procedures." $n = 4$–5/group. Results shown are mean ± S.E. (*error bars*). *, $p < 0.05$ by *t* test; *n.s.*, not significant. *F*, CaCo2 cells that did or did not overexpress SLC30A10 WT were differentiated for 4 weeks. Subsequently, the manganese pulse-chase assay was performed, and metal levels were analyzed as described under "Experimental procedures." $n = 5$/group. Results shown are mean ± S.E. *, $p < 0.05$ by one-way ANOVA and Tukey Kramer post hoc test.

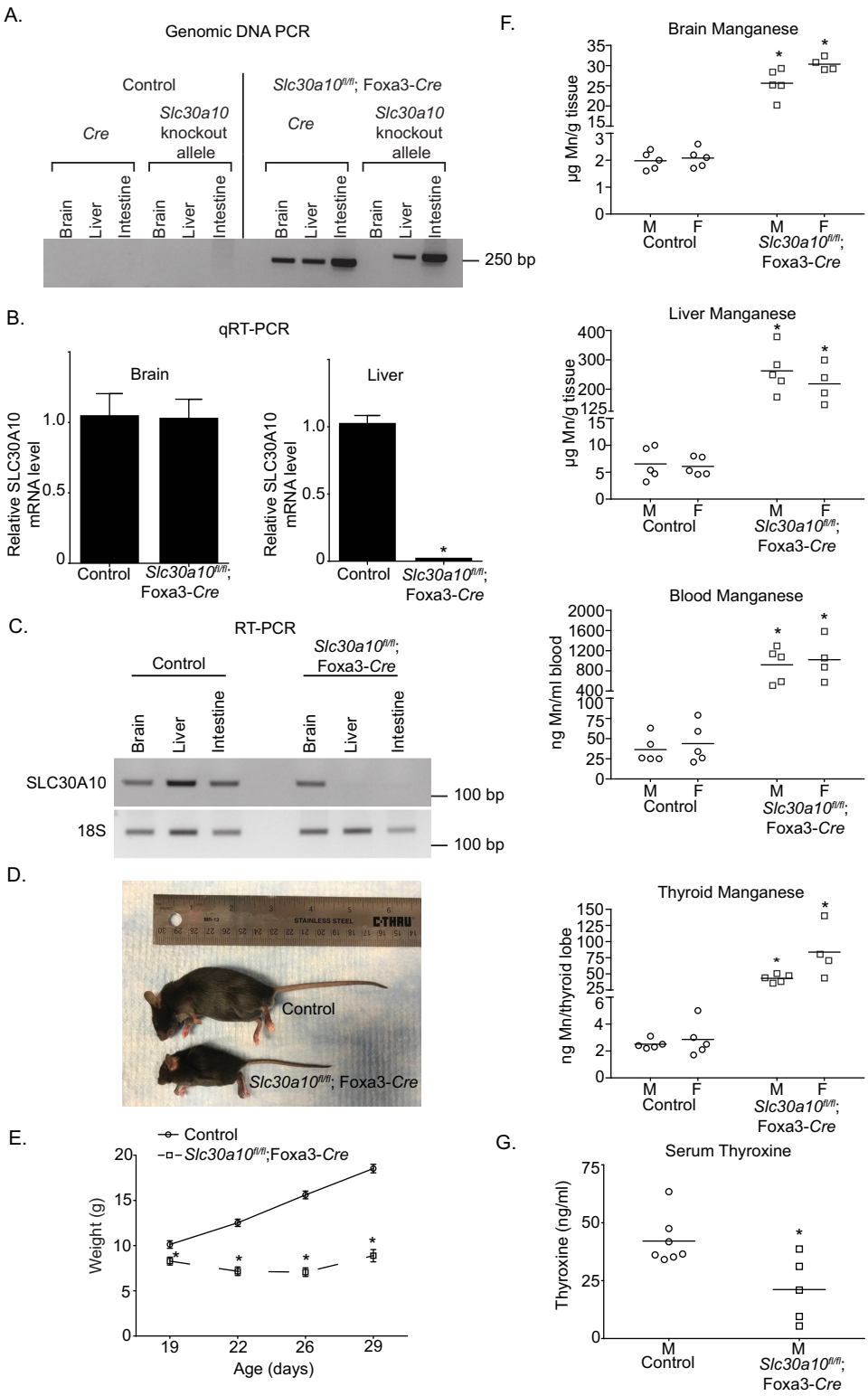

Figure 5. Endoderm-specific *Slc30a10* knockouts have marked elevations in tissue manganese levels and develop severe manganese toxicity. *A*, PCR assays were performed to detect the recombined *Slc30a10* allele and the *Cre* transgene. *B*, qRT-PCR assays were performed to quantify SLC30A10 mRNA levels in control or endoderm-specific knockouts. $n = 3$/group. Results shown are mean ± S.E. (*error bars*). *, $p < 0.05$ by *t* test. *C*, RT-PCR assays were performed to detect SLC30A10 and 18S mRNA in brain, liver, or intestines. *D*, photograph of a 6-week-old male knockout and its male littermate control. *E*, body weights of male controls or knockouts. Only males were used because our prior work showed that, in whole-body knockouts, deficiency in body weight was more severe in males (22). In this study, assays in a few animals revealed that body weights of female endoderm-specific knockouts were also lower than sex-matched controls. $n = 12$ controls and 8 knockouts. Results shown are mean ± S.E. (*error bars*). *, $p < 0.05$ by repeated measures two-way ANOVA and Sidak's post hoc test. *F*, tissue manganese levels were measured in 6-week-old control or knockout mice. $n = 5$ males and 5 females for control and 5 males and 4 females for knockouts. *Line*, mean. *, $p < 0.05$ by two-way ANOVA and Sidak's post hoc test for differences between genotypes compared in a sex-specific manner. *G*, serum thyroxine levels of 6-week-old male control or knockouts. Only males were used because earlier work in whole-body *Slc30a10* knockouts revealed that hypothyroidism was more severe in males (22). $n = 7$ controls and 5 knockouts. *Line*, mean. *, $p < 0.05$ by *t* test.

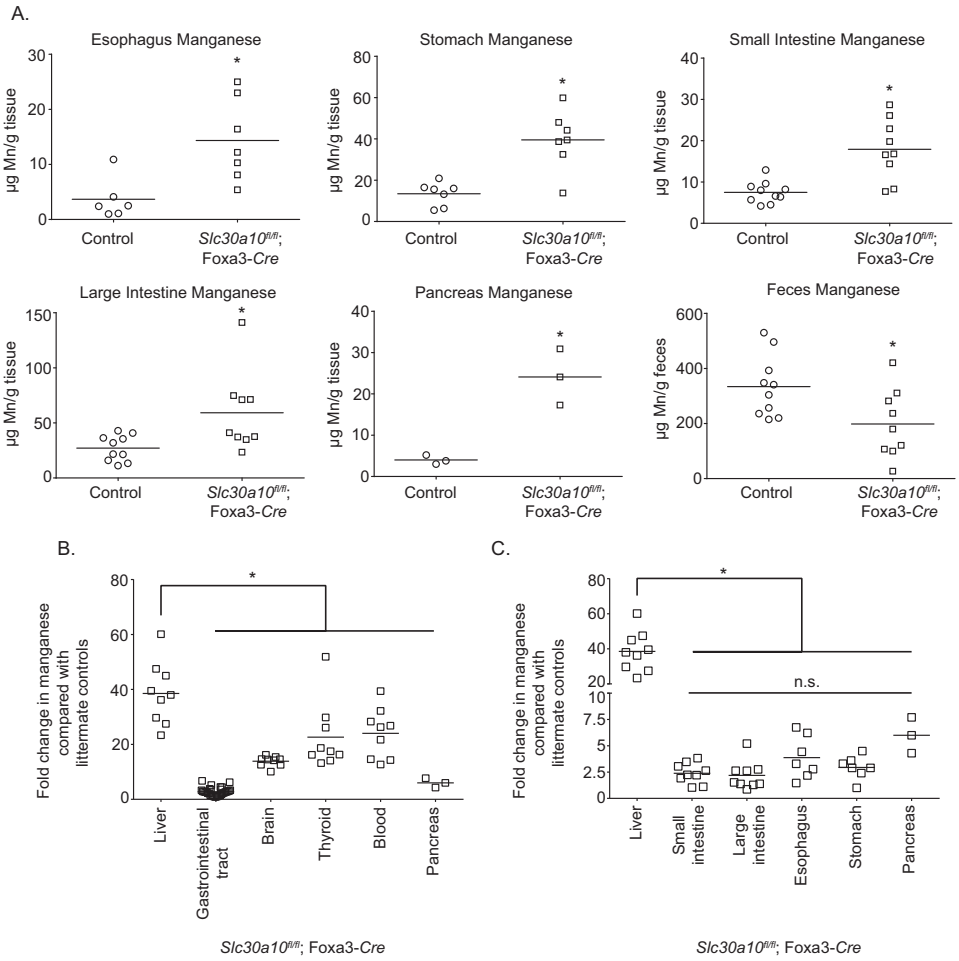

Figure 6. Manganese levels are enhanced in the gastrointestinal tract of endoderm-specific *Slc30a10* knockouts, but the extent of elevation is greater in the liver. *A*, manganese levels were measured in the indicated tissues isolated from 4–6-week-old endoderm-specific knockouts or littermate controls. For intestines and feces, $n = 5$ males and 5 females for control and 5 males and 4 females for knockouts. For esophagus, $n = 2$ males and 4 females for control and 4 males and 3 females for knockouts. For stomach, $n = 2$ males and 5 females for control and 4 males and 3 females for knockouts. For pancreas, $n = 3$ males per genotype. Sexes were combined for analyses to increase statistical power as effect sizes were small. *Line*, mean. *, $p < 0.05$ by *t* test. *B* and *C*, comparison of the -fold change in manganese levels in indicated organs of endoderm-specific knockouts relative to littermate controls from Fig. 5*F* and *A* above. Sexes were combined to increase power, as effect sizes in the gastrointestinal tract were small. *Line*, mean. For *B*, data from the esophagus, stomach, and intestines were pooled into the "gastrointestinal tract" group. For *B*, *, $p < 0.05$ by one-way ANOVA and Dunnett's post hoc test for the comparison between liver and other organs. For *C*, *, $p < 0.05$ by one-way ANOVA and Tukey–Kramer post hoc test for the comparison between liver and other organs. *n.s.*, there were no significant differences between extrahepatic organs in *C* by one-way ANOVA and Tukey–Kramer post hoc test.

Slc30a10$^{fl/fl}$;Foxa3-*Cre* animals were hypothyroid. Elevations in manganese levels were also evident in the walls of the esophagus, stomach, and small and large intestines of the endoderm-specific knockouts (Fig. 6*A*). Notably, the liver accumulated substantially more manganese than the gastrointestinal tract and other organs (Fig. 6, *B* and *C*), consistent with its role as the primary organ that excretes manganese. Further, within the digestive system, the extent of manganese accumulation in the esophagus, stomach, intestines, and pancreas was comparable (Fig. 6*C*). Finally, fecal manganese levels of the endoderm-specific knockouts were ~40% lower than littermate controls (Fig. 6*A*), congruent with the idea that excretion of manganese was reduced. Only minor changes were evident in levels of other metals (Figs. S4–S6); these were likely secondary to changes in manganese.

To determine whether the phenotypic changes observed in *Slc30a10*$^{fl/fl}$;Foxa3-*Cre* mice were induced by manganese toxicity, we performed a rescue experiment that involved changing the diet to one that had a lower amount of manganese (see "Experimental procedures"). Our prior work with the whole-body knockouts revealed that manganese in regular rodent chow (~84 μg of manganese/g of chow; PicoLab Rodent Diet 20) was the source of toxicity. Changing the diet to reduced manganese (~11 μg of manganese/g of chow; AIN-93G) lowered tissue manganese levels and rescued the failure-to-thrive and hypothyroidism phenotype (22). In the current study, at 6 weeks of age, manganese levels in the brain, liver, and thyroid of *Slc30a10*$^{fl/fl}$;Foxa3-*Cre* mice on the reduced manganese diet were still greater than littermate controls (Fig. 7*A*). Importantly, however, manganese levels of the endoderm-specific knockouts on the reduced manganese diet were significantly lower than those that had been fed regular rodent chow (Fig. 7*B*). The reduced manganese diet did not alter tissue manganese levels of littermate controls (Fig. 7*B*). Additionally, the reduced manganese diet did not alter levels of zinc, iron, or copper in control or endoderm-specific knockouts (Fig. S7).

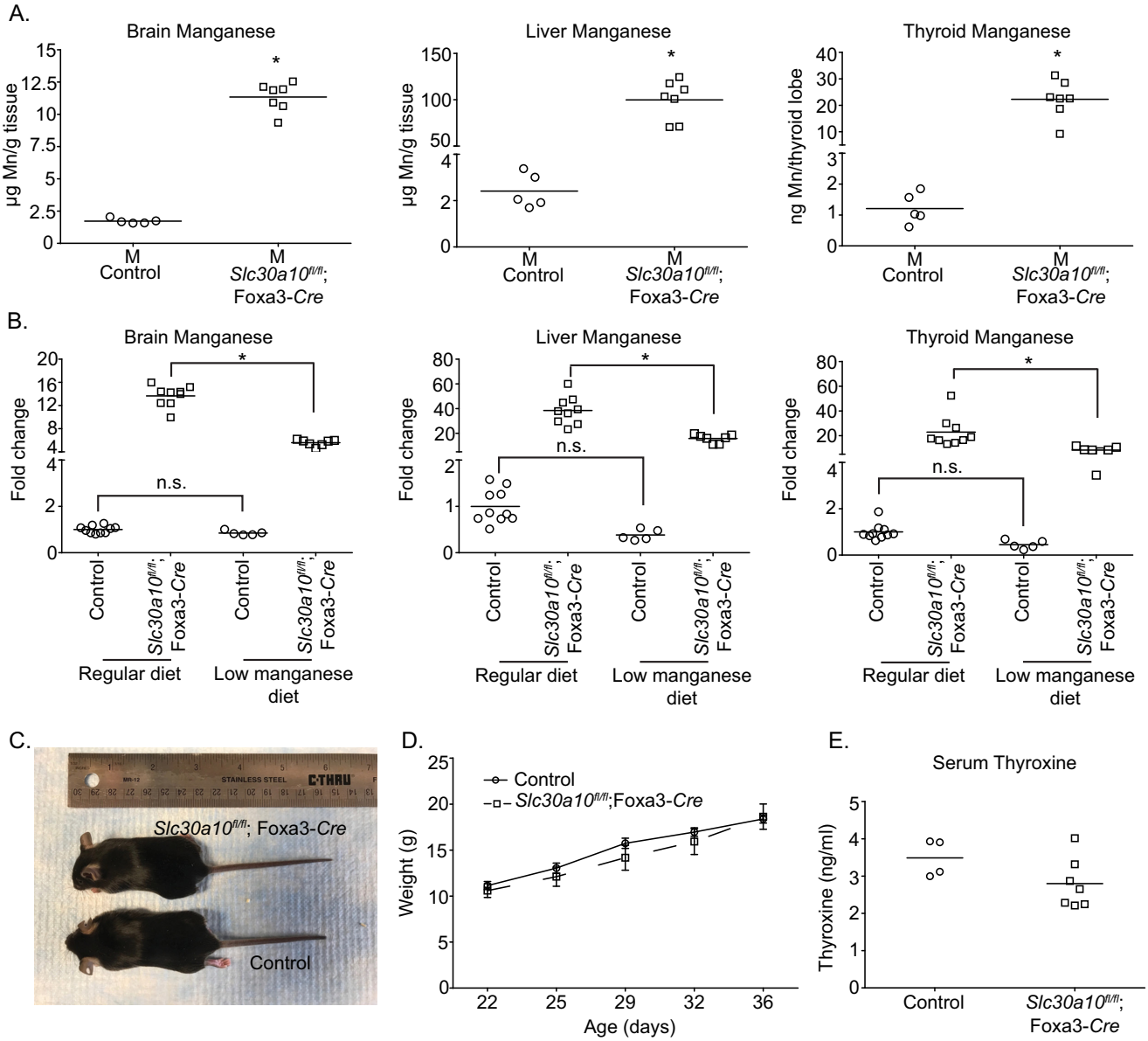

Figure 7. A reduced manganese diet rescues the phenotype of endoderm-specific *Slc30a10* knockouts. *A*, tissue manganese levels were measured in 6-week-old control or endoderm-specific knockout mice fed the reduced manganese diet. Only males were used for the rescue assay because data in Fig. 5 showed that male endoderm-specific knockouts developed severe toxicity, and prior work in whole-body knockouts demonstrated that manganese-induced phenotypic changes were more severe in males (22). $n = 5$ controls and 7 knockouts. *Line*, mean. *, $p < 0.05$ by *t* test. *B*, comparison of the -fold change in tissue manganese levels of animals in *A* above relative to mice on regular rodent chow in Fig. 5*F*. For each tissue, mean manganese levels of controls fed regular chow were normalized to 1. For animals from Fig. 5*F*, sexes were combined. *Line*, mean. *, $p < 0.05$ by one-way ANOVA and Tukey–Kramer post hoc test. *n.s.*, not significant. *C*, photograph of a 6-week-old male knockout and its male littermate control. *D*, body weights of male controls or knockouts. $n = 9$ controls and 7 knockouts. Results shown are mean ± S.E. (*error bars*). There were no differences between groups at any time point using repeated measures two-way ANOVA and Sidak's post hoc test. *E*, serum thyroxine levels of 6-week-old male controls or knockouts. $n = 4$ controls and 7 knockouts. *Line*, mean. There were no genotype-specific differences using *t* test.

Overall, the diet specifically reduced manganese levels in the endoderm-specific knockouts. Notably, body weights and serum thyroxine levels of *Slc30a10*$^{fl/fl}$;Foxa3-*Cre* mice on the reduced manganese diet were comparable with littermate controls (Fig. 7, *C–E*). Thus, similar to the whole-body knockouts, the decrease in body weight and thyroid dysfunction observed in endoderm-specific *Slc30a10* knockouts is also a consequence of manganese toxicity. Results of Figs. 2–7, taken together, imply that, under basal conditions, manganese levels in the brain as well as in other organs in the body are regulated by the activity of SLC30A10 in the digestive system.

Whole-body, but not endoderm-specific, Slc30a10 knockouts develop manganese-induced neuromotor deficits

Intriguingly, mean brain manganese levels of the endoderm-specific knockouts on the regular diet analyzed in Fig. 5 (28 μg of manganese/g of tissue) were lower than that of whole-body knockouts analyzed in Fig. 1 (41 μg of manganese/g of tissue; $p < 0.05$). However, mean liver manganese levels of the two

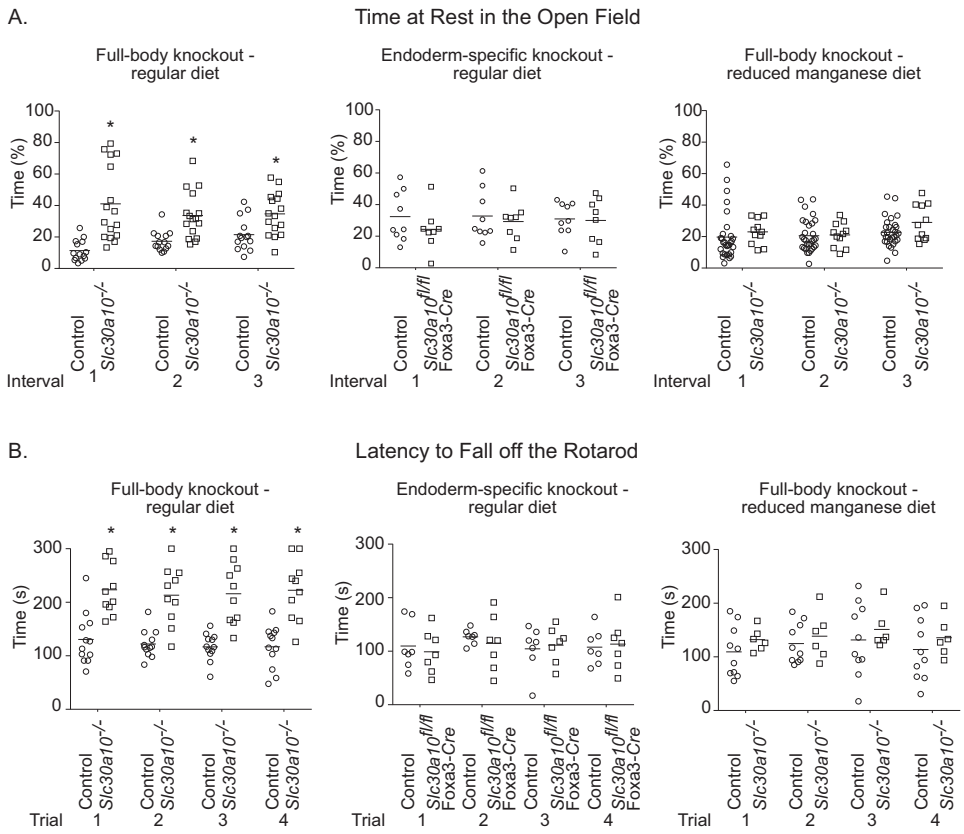

Figure 8. Whole-body, but not endoderm-specific, *Slc30a10* knockout mice exhibit manganese-induced motor dysfunction. *A*, depiction of the percentage of time animals spent at rest in the open-field test. Animals on regular diet were analyzed at 5–6 weeks of age. Analyses at later time points were not possible because animals died between 7 and 8 weeks of age. Those on the reduced manganese diet were analyzed at 7–10 weeks of age. For whole-body knockouts on regular diet, $n = 7$ male and 7 female controls and 9 male and 7 female knockouts. For the endoderm-specific knockouts, $n = 4$ male and 5 female controls and 4 male and 4 female knockouts. For the whole-body knockouts on the reduced manganese diet, $n = 16$ male and 14 female controls and 6 male and 5 female knockouts. Sexes were combined for analyses to increase statistical power and because strong sex-specific differences were not observed. *Line*, mean. *, $p < 0.05$ by repeated measures two-way ANOVA and Sidak's post hoc test. *B*, latency of animals to fall off the rod was calculated after performance of the rotarod test. The test was performed at the same age as the open-field test above. For whole-body knockouts on regular diet, $n = 6$ male and 6 female controls and 5 male and 5 female knockouts. For the endoderm-specific knockouts, $n = 3$ male and 4 female controls and knockouts. For the whole-body knockouts on the reduced manganese diet, $n = 5$ male and 5 female controls and 3 male and 3 female knockouts. Sexes were combined for analyses to increase statistical power and because robust sex-specific differences were not observed. *Line*, mean. *, $p < 0.05$ by repeated measures two-way ANOVA and Sidak's post hoc test.

knockout strains were comparable ($p > 0.05$). Additionally, there were no differences between brain or liver manganese levels of the littermate controls for the two strains ($p > 0.05$). Thus, differences in brain manganese levels of the two knockout strains were unlikely to be a consequence of genetic background. The major distinction between the whole-body and endoderm-specific knockouts is that expression of SLC30A10 is depleted in the brain of the whole-body knockouts only. This observation raised the hypothesis that activity of SLC30A10 in the brain may, in fact, reduce brain manganese when manganese levels increase in the body to protect against neurotoxicity.

As the first test of this hypothesis, we assayed for the neurobehavioral function of whole-body and endoderm-specific knockouts using the open-field and rotarod tests when animals were fed regular rodent chow. For both tests, we initially compared differences between groups at 5–6 weeks of age, when phenotypic changes were clearly established in both knockout strains. Notably, compared with littermate controls, the whole-body knockouts spent more time at rest in the open-field test (Fig. 8*A*), suggesting reduced desire to explore and/or generalized changes in movement. On the rotarod, whole-body knockouts took more time to fall off the rod compared with littermate controls (Fig. 8*B*), suggesting altered ambulatory coordination or activity. Importantly, performance of the endoderm-specific knockouts in both tests was comparable with littermate controls (Fig. 8, *A* and *B*). Moreover, neurobehavioral changes observed in the whole-body knockouts were rescued when the animals were placed on a reduced manganese diet (Fig. 8, *A* and *B*), implying that manganese toxicity was the cause. Note that the defects in neurobehavior observed in the whole-body knockouts could not be a consequence of their smaller body size or thyroid dysfunction, because the endoderm-specific knockouts were also hypothyroid and had substantial reductions in body size/weight. For added rigor, we repeated the above experiment at two additional earlier time points, postnatal days 24–26 and 28–30, when phenotypic changes are developing in both whole-body and endoderm-specific knockouts. The trend for the whole-body, but not endoderm-specific, knockouts to spend more time at rest in the open-field test and take more time to fall off the rod on the rotarod test was also evident at these earlier time points (Figs. S8 and S9). Taken together, these data suggest that whole-body knockouts have

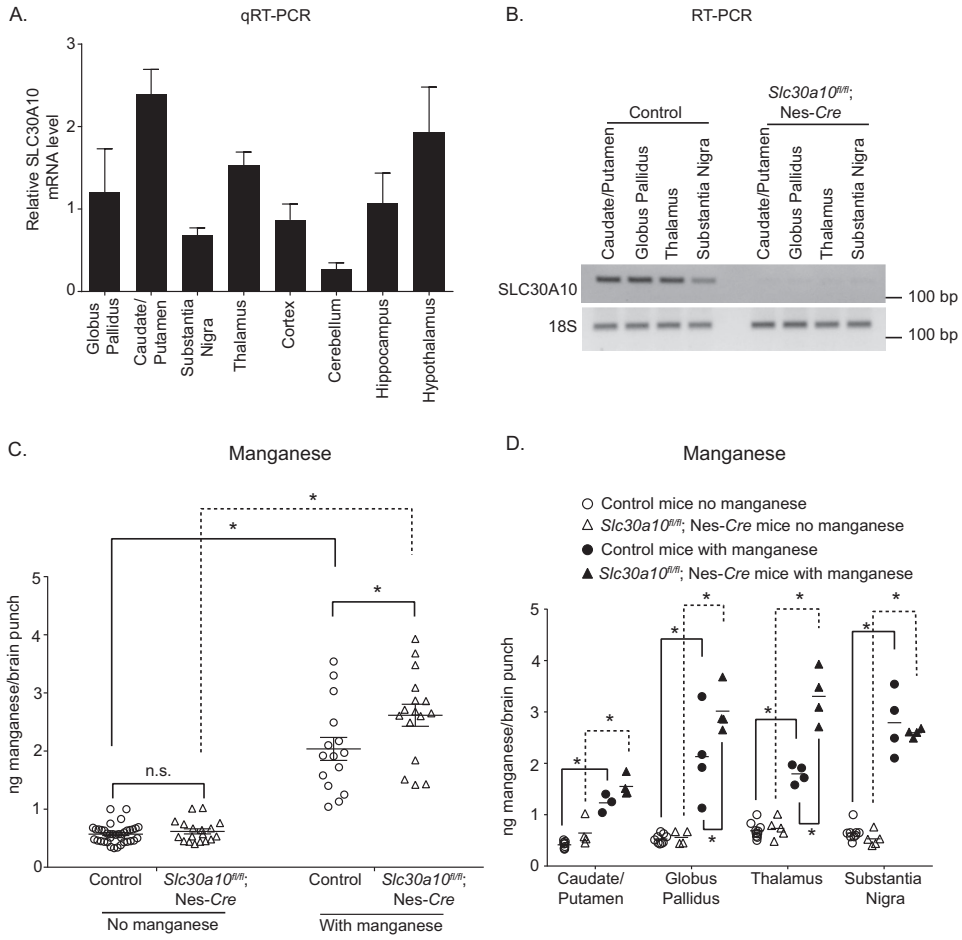

Figure 9. Following manganese exposure, manganese levels are elevated in specific brain regions of pan-neuronal/glial *Slc30a10* knockout mice. *A*, qRT-PCR analyses were performed to assay for SLC30A10 mRNA levels in the indicated brain regions of WT mice. $n = 3$. Results shown are mean ± S.E. (*error bars*). *B*, RT-PCR analyses were performed to detect SLC30A10 and 18S mRNA in the indicated brain regions of pan-neuronal/glial knockouts or littermate controls. *C* and *D*, manganese levels were measured in the caudate/putamen, globus pallidus, thalamus, and substantia nigra of pan-neuronal/glial knockouts or littermate controls treated with or without subcutaneous manganese as described under "Experimental procedures." $n = 10$ mice for controls without manganese, 5 for knockouts without manganese, and 4 each for controls or knockouts with manganese. For *C*, data from all regions were pooled to increase power. For *C*, $n = 37$, 18, 15, and 16 samples for controls or knockouts without or with manganese treatment, respectively. For *D*, per brain region, $n = 9–10$, 4–5, 3–4, and 4 samples for controls or knockouts without or with manganese treatment, respectively. *Line*, mean. *, $p < 0.05$ using two-way ANOVA and Tukey–Kramer post hoc test; *n.s.*, not significant.

higher brain manganese levels than endoderm-specific knockouts and, therefore, develop manganese-induced functional alterations in neurobehavior.

After elevated manganese exposure, manganese levels in specific brain regions of pan-neuronal/glial Slc30a10 knockouts are enhanced

To definitively determine whether expression of SLC30A10 in the brain was neuroprotective when manganese levels increase in the body, we sought to compare brain manganese levels of the pan-neuronal/glial *Slc30a10* knockouts and their littermate controls after exposure to elevated manganese. We performed this experiment using four groups of animals: littermate controls or pan-neuronal/glial knockouts treated with or without 15 mg of manganese/kg of body weight delivered subcutaneously three times a week for 4 weeks starting at 2 months of age. Prior studies show that this dosing regimen is a suitable model to mimic sub-chronic manganese exposure that occurs in humans; mice exposed to this regimen exhibit modest increases in brain manganese levels (36). To enhance the strength of the experiment, instead of measuring brain manganese levels using a part of the midbrain as performed for other assays in this study, we used a brain punching method to collect tissue from the caudate/putamen, globus pallidus, and substantia nigra (all subregions within the basal ganglia) and the thalamus. This was important because manganese is known to induce injury in the basal ganglia and the thalamus (2, 3, 37). We verified that SLC30A10 was expressed in these brain regions in WT mice (Fig. 9*A*). We also verified that expression of SLC30A10 was depleted in these regions in the pan-neuronal/glial knockouts (Fig. 9*B*).

To increase statistical power, in the first round of analyses, we combined data from the four brain regions. In the absence of manganese treatment, there were no genotype specific differences in manganese levels (Fig. 9*C*). Within each genotype, treatment with manganese increased manganese levels (Fig. 9*C*). In the littermate control group, the manganese treatment regimen induced an ~3-fold increase in manganese levels (Fig. 9*C*). This modest increase was similar to the ~2–3-fold increase in brain manganese levels reported in human patients

suffering from manganese neurotoxicity due to elevated exposure (38), validating the disease relevance of our exposure regimen. Importantly, after manganese treatment, manganese levels in the pan-neuronal/glial knockouts were higher than littermate controls (Fig. 9*C*). The observed changes were specific because there was no effect of genotype or manganese treatment on zinc, iron, or copper levels (Fig. S10).

Subsequently, we separated the data by brain region and repeated the statistical analyses. In the absence of manganese treatment, there were no differences in manganese levels between genotypes in any region (Fig. 9*D*). Treatment with manganese increased manganese levels within each genotype in each brain region (Fig. 9*D*). Notably, after manganese treatment, manganese levels in the globus pallidus and thalamus of the pan-neuronal/glial knockouts were higher than littermate controls (Fig. 9*D*). A trend toward an increase was also evident in the caudate/putamen (Fig. 9*D*), but there was no effect of manganese treatment between genotypes in the substantia nigra (Fig. 9*D*). Overall, with exposure to elevated manganese, depletion of SLC30A10 in the brain leads to an increase in manganese levels in specific brain regions. In sum, results of Figs. 8 and 9 and Figs. S8–S10, taken together, indicate that expression of SLC30A10 in the brain lowers brain manganese when levels increase in the body and thereby protects against neurotoxicity.

Discussion

At the start of this study, we anticipated that brain manganese levels would be regulated by activity of SLC30A10 in the brain and/or the liver. Instead, we made the surprising discovery that, under basal physiological conditions, brain manganese is regulated by the activity of SLC30A10 in the entire digestive system, and not the brain or exclusively the liver. An important implication is that alterations in SLC30A10 activity in the digestive system may modulate neurological outcomes of manganese toxicity. Currently, there are no treatments for manganese neurotoxicity. A particular challenge is to generate drugs that cross the blood–brain barrier. Our work raises the possibility that drugs that enhance levels or activity of SLC30A10 in the digestive system may increase manganese excretion and thereby reduce the body burden of manganese. Such drugs could be therapeutically beneficial without having to reach the brain.

Excretion by the liver is the main route of manganese elimination (6–10). However, transport of manganese into bile is saturable (9, 10), and there is historical evidence for the excretion of manganese by the gastrointestinal tract (6, 8). In 1943, Greenberg *et al.* (7) reported that radiotracer manganese was primarily excreted in bile in rats, but a pool of manganese also accumulated in the gastrointestinal tract. Importantly, in 1966, Papavasiliou *et al.* (8) demonstrated that bile duct ligation robustly inhibited the excretion of radiotracer manganese in rats, but manganese excretion in duct-ligated animals could be enhanced by provision of supplemental manganese, and a rectal ligation was necessary to completely abolish manganese excretion. Consistent with the above study, also in 1966, Bertinchamps *et al.* (6) provided direct evidence for the excretion of radiotracer manganese by segments of the small intestines in rats; these authors further reported that rats consuming a high-manganese diet responded to a parenteral manganese load by increasing the excretion of manganese through the intestines, whereas those on a low-manganese diet responded to a similar challenge by increasing biliary excretion. The totality of evidence suggests that parts of the gastrointestinal tract (*e.g.* intestines) play a critical role in excreting manganese when transport into bile is compromised or saturated. Our current findings, showing that body manganese levels were substantially elevated when SLC30A10 was depleted both in the liver and the gastrointestinal tract, but not just the liver, fit well with these prior studies.

In 2016, loss-of-function mutations in another manganese transporter, SLC39A14, were reported to cause manganese-induced neurotoxicity in humans (39). SLC39A14 has the capability to mediate manganese influx (20). In humans harboring mutations in *SLC39A14*, and in whole-body *Slc39a14* knockout mice, manganese levels in several extrahepatic organs (*e.g.* brain), but not the liver, were elevated (23, 39–42). Additionally, SLC39A14 localized to the basolateral aspect of hepatocytes (23, 43). These findings indicate that SLC39A14 plays a critical role in the transport of manganese from the circulation into the liver, and loss-of-function of SLC39A14 induces manganese toxicity by blocking hepatic manganese excretion. In a recent study, we compared the phenotypes of whole-body *Slc30a10* or *Slc39a14* single knockout mice with *Slc30a10*/*Slc39a14* double knockouts and reported that SLC39A14 and SLC30A10 cooperatively regulate hepatic manganese excretion; SLC39A14 transports manganese from blood into hepatocytes, and SLC30A10 subsequently excretes the intrahepatic manganese (20, 23).

Interestingly, body manganese levels did not increase in liver-specific *Slc39a14* knockouts (42), suggesting that extrahepatic components of the digestive system compensate for the loss of function of SLC39A14 in the liver as well. Notably, SLC39A14 was also detected in the intestines and localized to the basolateral aspect of enterocytes (44). Further, whole-body *Slc39a14* knockouts did not accumulate manganese in the intestines (42), implying that SLC39A14 is required for import of manganese into intestinal enterocytes. Thus, in addition to the liver, SLC39A14 and SLC30A10 may act in a coordinated manner to mediate manganese excretion via the gastrointestinal tract as well.

Our results indicate that, when manganese levels increase in the body, activity of SLC30A10 in the brain becomes important to reduce manganese and protect against neurotoxicity. The first line of evidence in support of the above idea comes from the fact that manganese levels in the brain, but not the liver, of the endoderm-specific knockouts were lower than whole-body knockouts, and only whole-body knockouts developed manganese-induced neurobehavioral deficits. In prior studies, WT rodents exposed to elevated manganese exhibited reduced movement in the open-field test (36, 45, 46) and had a lower latency to fall off the rotarod (45, 47, 48). Reduced movement of the whole-body *Slc30a10* knockouts in the open-field test observed here is consistent with prior work. In contrast, whole-body *Slc30a10* knockouts took a longer time to fall off the rotarod. The reasons for the divergence in results of the rotarod

assay are unclear. One possibility is that manganese toxicity in early life induces complex changes in attention, activity, and motor function (49, 50). In whole-body *Slc30a10* knockouts, unlike WT animals, homeostatic control of manganese in the brain may be altered from birth in a manner that affects performance on the rotarod test. Two additional points are worth noting in this discussion. Whole-body *Slc39a14* knockouts also had a lower latency to fall off the rotarod (41, 42). However, *Slc39a14* knockouts develop torticollis (41, 42, 51), which makes it challenging to directly compare their performance in neurobehavioral assays with other strains. Finally, genetic backgrounds of mice influence performance in neurobehavioral tests (52). The hybrid background of our strains may have impacted their sensitivity to developing manganese-induced neurobehavioral deficits.

In manganese-treated animals, levels of manganese in the globus pallidus and thalamus of pan-neuronal/glial knockouts were ~50–80% greater than littermate controls. This result further supports the idea that activity of SLC30A10 in the brain is neuroprotective when manganese levels increase in the body. The observed difference between genotypes is biologically relevant because, in humans, an ~2–3-fold increase in brain manganese induces neurotoxicity (38) (estimated human brain manganese levels are ~5–14 ng/mg protein or 20–53 μM in physiologic conditions and 16–42 ng/mg protein or 60–158 μM in disease (38)). Notably, the globus pallidus is particularly sensitive to manganese accumulation and induced injury (2, 3). The thalamus is also a known manganese target (37). The reason why activity of SLC30A10 is critical to regulate manganese levels in these regions remains to be elucidated. Future analyses of mice that lack SLC30A10 expression only in neurons in these regions should provide fundamental insights into the mechanisms of manganese neurotoxicity.

As with most studies, our work also has limitations. As mentioned previously, lack of a specific antibody precluded inclusion of assays documenting loss of SLC30A10 protein in our knockout strains. However, we robustly validated each strain using PCR, RT-PCR, and qRT-PCR, and the absence of protein-based data is not expected to confound interpretation. Further, in addition to manganese, several other nutrients vary between regular rodent chow (PicoLab Rodent Diet 20) and the reduced manganese diet (AIN-93G). Notably, the reduced manganese diet lowered tissue manganese, but not zinc, iron, or copper, levels in the endoderm-specific knockouts, but not littermate controls. Thus, in terms of these major essential metals, the effect of the diet was specific to manganese, justifying its use as a means to lower manganese levels in the knockouts. The unlikely possibility that other nutrients in the reduced manganese diet impact the phenotype of mice lacking SLC30A10 remains to be investigated.

In sum, we show that activity of SLC30A10 in the entire digestive system, not just the liver, regulates brain manganese under basal conditions. Activity in the brain protects against neurotoxicity when body manganese levels increase. These results enhance understanding of the homeostatic regulation of manganese as well as the pathobiology of manganese-induced neurotoxicity at the organism level.

Experimental procedures

Generation and housing of knockout strains

All experiments with mice were approved by the Institutional Animal Care and Use Committee of the University of Texas (Austin, TX). We recently described generation of homozygous floxed *Slc30a10* mice (*Slc30a10*$^{fl/fl}$) in which exon 1 of *Slc30a10* was flanked by *loxP* sites (22). Exon 1 codes for amino acids 1–205 of mouse SLC30A10, which encompass most of the transmembrane domain required for manganese transport (21, 22). To briefly summarize here, the targeting vector was electroporated into V6.5 embryonic stem cells (C57BL/6 × 129S4/SvJae) (22). Germ-line chimeras were crossed with WT C57BL/6J mice, obtained from the Jackson Laboratory (Bar Harbor, ME), to generate mice heterozygous for the floxed allele, and heterozygous floxed mice were intercrossed to produce homozygous floxed animals (22). *Slc30a10*$^{fl/fl}$ mice were on a hybrid C57BL/6 × 129S background.

We also described generation of whole-body *Slc30a10* knockouts by crossing *Slc30a10*$^{fl/fl}$ mice with the Sox2-*Cre* strain (Jackson Laboratories strain 008454; C57BL/6J background) (22). Whole-body knockouts are referred to as *Slc30a10*$^{-/-}$ mice here and were maintained on a hybrid C57BL/6 × 129S background. Littermates of the whole-body knockouts (*Slc30a10*$^{+/+}$ or *Slc30a10*$^{+/-}$ genotypes) are phenotypically indistinguishable from each other (22). Therefore, littermates were combined into a control group for comparisons with *Slc30a10*$^{-/-}$ mice.

For generation of tissue-specific knockout mice, we obtained Nes-*Cre* (strain number 003771; C57BL/6J background) and Alb-*Cre* (strain number 003574; C57BL/6J background) mice from the Jackson Laboratories. For the Foxa3-*Cre* strain, we obtained cryopreserved sperm for heterozygous males (Tg(Foxa3-*Cre*)1Khk/Mmmh; CD1 background) from the Mutant Mouse Regional Resource Center, a National Institutes of Health–funded strain repository. The strain was recovered by *in vitro* fertilization (53) at the Mouse Genetic Engineering Facility of the University of Texas (Austin, TX) using oocytes from C57BL/6J female mice. To obtain each tissue-specific knockout strain, we crossed *Slc30a10*$^{fl/fl}$ mice with animals expressing the *Cre* transgene. Progeny that were heterozygous for the floxed *Slc30a10* allele and that also expressed *Cre* were again crossed with *Slc30a10*$^{fl/fl}$ mice to produce the tissue-specific knockouts, which were homozygous for the floxed *Slc30a10* allele and positive for expression of *Cre*. The tissue-specific knockouts are designated as *Slc30a10*$^{fl/fl}$;Nes-*Cre* (pan-neuronal/glial knockouts), *Slc30a10*$^{fl/fl}$;Alb-*Cre* (liver-specific knockouts), or *Slc30a10*$^{fl/fl}$;Foxa3-*Cre* (endoderm-specific knockouts). Similar to the whole-body knockouts, *Slc30a10*$^{fl/fl}$;Nes-*Cre* and *Slc30a10*$^{fl/fl}$;Alb-*Cre* mice were on a hybrid C57BL/6 × 129S background. *Slc30a10*$^{fl/fl}$;Foxa3-*Cre* mice were on a hybrid C57BL/6 × 129S × CD1 background.

The breeding strategy for the tissue-specific knockouts produced littermates that were homozygous for the unrecombined floxed allele or heterozygous for the recombined or unrecombined floxed allele. There were no phenotypic differences in tissue manganese levels, body size or weight, or neurobehavior between mice of these genotypes. Therefore, for each knockout

strain separately, littermates were combined into a control group. Analyses were performed between knockout strains and their respective littermate controls.

Animals were housed in the conventional or specific pathogen-free facility of the University of Texas (Austin, TX) in a room maintained at ~21 °C with a 12-h light–dark cycle. After weaning, 2–5 littermates of the same sex were kept per cage. Animals had free access to food and water. The regular diet was PicoLab Rodent Diet 20, which contains ~84 μg of manganese/g of chow. The low-manganese diet was AIN-93G with ~11 μg of manganese/g of chow. For the diet change rescue experiment, diet was changed to reduced manganese on postnatal day 10, as described by us previously for whole-body knockouts (22). Intake of food was comparable between the diets.

PCR, RT-PCR, and genotyping

For genotyping live animals, genomic DNA was isolated from samples of ear punches or tail snips as described by us previously (22, 23). PCR was performed to amplify *Slc30a10* alleles (WT, floxed, or recombined) and the *Cre* transgene using primers and PCR conditions described previously (22, 23). For validation of the genotype, mice were euthanized by decapitation following isoflurane (Piramal Enterprises, Mumbai, India) anesthesia. Tissue samples were dissected and flash-frozen in liquid nitrogen. For PCR, genomic DNA was isolated from tissue, and PCR was performed to amplify the recombined *Slc30a10* allele and the *Cre* transgene using primers and conditions described earlier (22, 23). For RT-PCR, RNA was extracted and reverse-transcribed into cDNA as described previously (19). PCR was then performed to amplify *Slc30a10* and *18S* gene products using primers and PCR conditions described previously (22, 23).

Quantitative RT-PCR

For qRT-PCR, mice were euthanized by decapitation as described above. RNA samples were generated and reverse-transcribed to cDNA also as described above. Quantitative RT-PCR was performed as described previously (19, 23). Transcript levels were quantified using the $\Delta\Delta C_T$ method with 18S as internal control (54).

Analyses of metal and serum thyroxine levels in mice

Tissue metal levels were analyzed using inductively coupled plasma MS, and thyroxine levels were assayed using the Accu-Diag T4 ELISA kit (Diagnostic Automation/Cortex Diagnostics, Inc., Woodland Hills, CA) exactly as described in our recent publications (22, 23). Other than in the brain punch experiment, a part of the midbrain was used to assay for brain metal levels.

Culture of undifferentiated CaCo2 cells and generation of a CaCo2 subline that overexpressed SLC30A10

CaCo2 cells were purchased from the ATCC (Manassas, VA). For undifferentiated cultures, cells were grown in Eagle's minimum essential medium (Corning, Corning, NY) supplemented with 10% fetal bovine serum (Atlanta Biologicals, Flowery Branch, GA), 100 IU/ml penicillin-G, and 100 μg/ml streptomycin (both from Corning). To generate the CaCo2 subline that overexpressed human SLC30A10, we infected cells with a lentivirus that included a third-generation transfer plasmid coding for FLAG-tagged human SLC30A10 WT as described by us recently (26). The transfer plasmid also conferred resistance to puromycin. Therefore, we grew the infected subline in the presence of 2 μg/ml puromycin.

Differentiation of CaCo2 cells

Differentiation was performed essentially as described (30). Briefly, cells were seeded onto polycarbonate filters that were 6.5 mm in diameter and that had a pore diameter of 0.4 μm (Corning). Filters were placed on inserts within wells of a 24-well plate such that the media bathing the apical and basal compartments were kept separated (Fig. S3*A*). Both compartments received minimum essential medium supplemented with 10% fetal bovine serum (100 μl in the apical and 500 μl in the basal compartment). Media were changed every 3 days, and cells were cultured for 4 weeks before analyses.

Measurement of intracellular metals in differentiated CaCo2 cells

Cells were treated with 12.5 μM manganese for 16 h. Manganese was added to the basal compartment. After this, cells were harvested by trypsinization. Further processing for metal measurements using inductively coupled plasma MS was as described by us previously (19).

Pulse-chase assay in differentiated CaCo2 cells

Cells were treated with manganese as described above (pulse phase). After this, cultures were washed five times with PBS. Then Hanks' balanced salt solution that did not contain manganese was added to both the basal and apical compartments (100 μl in the apical compartment and 500 μl in the basal compartment). Cells were then incubated at 37 °C for 1 h (chase phase). After the chase, Hanks' balanced salt solution added to the apical compartment was collected for metal analyses. Subsequently, cells were harvested as described above to assay for intracellular metal levels. Metal levels in both compartments were analyzed by inductively coupled plasma MS. The protocol for this pulse-chase experiment is essentially similar to that described by us for assays in HeLa cells previously (19).

Immunofluorescence assays in CaCo2 cells

Cells were fixed using 4% paraformaldehyde and processed for immunofluorescence as described previously (19, 21, 23, 55, 56). Undifferentiated CaCo2 cells were cultured and processed on glass coverslips. Before imaging, the coverslips were inverted onto glass slides and sealed using nail polish. Differentiated cells were cultured and processed on their polycarbonate filters. Before imaging, the filters were placed on glass slides such that the polycarbonate filters were on the slide. A glass coverslip was placed over the apical domain. The diameter of the coverslip was larger than the filter so that the filter was entirely encompassed by the coverslip. The coverslip was then sealed onto the glass slide using nail polish. We used an inverted microscope for imaging (see below), and the coverslip faced the objective.

Therefore, the polycarbonate filter did not interfere with the light path to the eyes or the camera.

Images were captured using a Nikon swept field confocal linked to an inverted Nikon TiE microscope equipped with a four-line high-power laser launch. The objective was a ×100, 1.45 numerical aperture oil-immersion objective (Nikon). The camera was an iXon3 X3 DU897 EM-CCD camera (Andor Technology). All images were captured as *z*-stacks with 0.5-μm spacing between individual frames. Images were processed using NIS Elements software.

Immunoblot assays

Immunoblots were performed exactly as described by us previously (19, 21)

Antibodies

We recently described the custom rabbit polyclonal antibody against the C-terminal domain of human SLC30A10 (23). This antibody specifically detects SLC30A10 in multiple different cell lines, including in HepG2 cells that we reported previously (23) and in intestinal CaCo2 cells used in this study. However, the antibody appears to lose specificity when mouse tissue samples are used. We have not been able to identify any commercial antibody that specifically detects SLC30A10 in rodent tissue. The mAb against tubulin (Sigma-Aldrich) was described previously (19, 21). Actin was detected using fluorescently labeled phalloidin (Thermo Fisher Scientific). Nuclei were demarcated using 4′,6-diamidino-2-phenylindole.

Chemicals

All chemicals were from Thermo Fisher Scientific or Sigma-Aldrich.

Brain microdissections

Whole brains were collected, flash-frozen in liquid nitrogen, and stored at −80 °C. Brains were embedded in Optimal Cutting Temperature Compound (Scigen Scientific, Gardena, CA), and frozen in cold isopentane (Thermo Fisher Scientific). They were then sliced on a cryostat (set to ∼−5 °C) in 500-μm sections. Sections were placed on microscope slides (∼3–4 sections per slide) and returned to dry ice to prevent thawing. Once all necessary sections were collected, slides were placed back in the cryostat (set to ∼−15 °C). Desired brain regions were identified using a mouse brain atlas and collected with a brain punching tool 1.25 mm in diameter (Stoelting Co., Wood Dale, IL). Two punches per region were collected. Tissue was not allowed to thaw during this process. Weights of punches from different regions and from animals of different genotypes were comparable.

Behavioral assessment

All behavior assays were conducted during the light hours of the light–dark cycle (7 a.m. to 7 p.m.). Numbers and age of testing for each assay are listed in the figure legends. For the open-field test, animals were individually placed in the center of the open-field chamber (Opto-Varimex 4 Activity Meter, Columbus Instruments, Columbus, OH), and activity was monitored for 15 min. Data were binned into 5-min intervals. The first 5-min trial is a test of the exploratory behavior of the animal in a novel environment, whereas subsequent trials provide information about general locomotor activity. The experimenter was not in the testing room while activity was monitored. After completion of the assessment, test animals were removed from the open-field chamber and returned to their home cages. The open-field chamber was cleaned with 5% ethanol between test animals.

For the rotarod test, animals were placed on an accelerating rotarod apparatus (Rotamex-5 Rota Rod, Columbus Instruments, Columbus, OH). The starting speed was 4 rpm and was increased by 0.6 rpm every 5 s for up to 300 s (40 rpm). Prior to each trial, animals were given a training session of ∼90 s at 4 rpm. Four trials were conducted with ∼20 min between each trial. Up to four animals were tested at a time. The apparatus was cleaned with 5% ethanol between animals and trials. Total time on the rod (latency to fall) was recorded.

Manganese treatment

For experiments in mice, a stock solution of 1.5 mg of manganese/ml of normal saline was prepared. All solutions were filtered prior to administration. Animals received subcutaneous injections at a final dose of 15 mg of manganese/kg of body weight. Injection volumes were ∼200–300 μl/animal. Vehicle-treated animals received only normal saline. Injections were initiated at 2 months of age and given three times a week for 4 weeks. After this, animals were euthanized for analyses. For experiments in cells, cultures were treated with a final concentration of 12.5 μM manganese in the form of $MnCl_2$.

Statistical analyses

Comparisons between multiple groups were performed using one- or two-way ANOVA and appropriate post hoc analyses. Comparisons between two groups were performed using Student's *t* test. For behavior and body weight analyses, which involved comparisons between multiple groups across multiple trials/time points, two-way ANOVA with repeated measures and appropriate post hoc tests were used. The PRISM 6 software (GraphPad Inc., La Jolla, CA) was used. For hypothesis testing, $p < 0.05$ was considered statistically significant. *Asterisks* in graphs denote statistically significant differences.

Author contributions—S. M. conceived the project and designed experiments with critical assistance from D. R. S. and C. A. T.; C. A. T., S. H., C. L., T. J., and W. S. performed experiments; C. A. T., S. M., and D. R. S. analyzed data; C. A. T. and S. M. generated figure panels; S. M. wrote the manuscript with critical contributions from C. A. T. and D. R. S.; and M. A. provided critical feedback on the paper.

Acknowledgments—We thank Dr. Nathaniel Miller (Jackson School of Geosciences, University of Texas, Austin, TX) for performing inductively coupled plasma MS assays in cell culture, Dr. Andrea C. Gore (College of Pharmacy, University of Texas, Austin, TX) for assistance with thyroxine measurement assays, and Dr. Yuri Bledrov and Dr. R. Adron Harris (Waggoner Center for Alcohol and Addiction Research, University of Texas, Austin, TX) for providing equipment to perform neurobehavior analyses.

References

1. Aschner, M., Erikson, K. M., Herrero Hernández, E., and Tjalkens, R. (2009) Manganese and its role in Parkinson's disease: from transport to neuropathology. *Neuromol. Med.* **11,** 252–266 CrossRef Medline
2. Olanow, C. W. (2004) Manganese-induced parkinsonism and Parkinson's disease. *Ann. N.Y. Acad. Sci.* **1012,** 209–223 CrossRef Medline
3. Perl, D. P., and Olanow, C. W. (2007) The neuropathology of manganese-induced Parkinsonism. *J. Neuropathol Exp. Neurol.* **66,** 675–682 CrossRef Medline
4. Lucchini, R. G., Guazzetti, S., Zoni, S., Benedetti, C., Fedrighi, C., Peli, M., Donna, F., Bontempi, E., Borgese, L., Micheletti, S., Ferri, R., Marchetti, S., and Smith, D. R. (2014) Neurofunctional dopaminergic impairment in elderly after lifetime exposure to manganese. *Neurotoxicology* **45,** 309–317 CrossRef Medline
5. Lucchini, R. G., Guazzetti, S., Zoni, S., Donna, F., Peter, S., Zacco, A., Salmistraro, M., Bontempi, E., Zimmerman, N. J., and Smith, D. R. (2012) Tremor, olfactory and motor changes in Italian adolescents exposed to historical ferro-manganese emission. *Neurotoxicology* **33,** 687–696 CrossRef Medline
6. Bertinchamps, A. J., Miller, S. T., and Cotzias, G. C. (1966) Interdependence of routes excreting manganese. *Am. J. Physiol.* **211,** 217–224 Medline
7. Greenberg, D. M., Copp, D. H., Cuthbertson, E. M. (1943) Studies in mineral metabolism with the aid of artificial radioactive isotopes: VII. The distribution and excretion, particularly by way of the bile, of iron, cobalt, and manganese. *J. Biol. Chem.* **147,** 749–756
8. Papavasiliou, P. S., Miller, S. T., and Cotzias, G. C. (1966) Role of liver in regulating distribution and excretion of manganese. *Am. J. Physiol.* **211,** 211–216 Medline
9. Ballatori, N., Miles, E., and Clarkson, T. W. (1987) Homeostatic control of manganese excretion in the neonatal rat. *Am. J. Physiol.* **252,** R842–R847 Medline
10. Klaassen, C. D. (1974) Biliary excretion of manganese in rats, rabbits, and dogs. *Toxicol. Appl. Pharmacol.* **29,** 458–468 CrossRef Medline
11. Butterworth, R. F. (2013) Parkinsonism in cirrhosis: pathogenesis and current therapeutic options. *Metab. Brain Dis.* **28,** 261–267 CrossRef Medline
12. Oulhote, Y., Mergler, D., Barbeau, B., Bellinger, D. C., Bouffard, T., Brodeur, M. È., Saint-Amour, D., Legrand, M., Sauvé, S., and Bouchard, M. F. (2014) Neurobehavioral function in school-age children exposed to manganese in drinking water. *Environ. Health Perspect.* **122,** 1343–1350 CrossRef Medline
13. Lechpammer, M., Clegg, M. S., Muzar, Z., Huebner, P. A., Jin, L. W., and Gospe, S. M., Jr. (2014) Pathology of inherited manganese transporter deficiency. *Ann. Neurol.* **75,** 608–612 CrossRef Medline
14. Quadri, M., Federico, A., Zhao, T., Breedveld, G. J., Battisti, C., Delnooz, C., Severijnen, L. A., Di Toro Mammarella, L., Mignarri, A., Monti, L., Sanna, A., Lu, P., Punzo, F., Cossu, G., Willemsen, R., *et al.* (2012) Mutations in SLC30A10 cause parkinsonism and dystonia with hypermanganesemia, polycythemia, and chronic liver disease. *Am. J. Hum. Genet.* **90,** 467–477 CrossRef Medline
15. Quadri, M., Kamate, M., Sharma, S., Olgiati, S., Graafland, J., Breedveld, G. J., Kori, I., Hattiholi, V., Jain, P., Aneja, S., Kumar, A., Gulati, P., Goel, M., Talukdar, B., and Bonifati, V. (2015) Manganese transport disorder: novel SLC30A10 mutations and early phenotypes. *Mov. Disord.* **30,** 996–1001 CrossRef Medline
16. Tuschl, K., Clayton, P. T., Gospe, S. M., Jr., Gulab, S., Ibrahim, S., Singhi, P., Aulakh, R., Ribeiro, R. T., Barsottini, O. G., Zaki, M. S., Del Rosario, M. L., Dyack, S., Price, V., Rideout, A., Gordon, K., Wevers, R. A., Chong, W. K., and Mills, P. B. (2012) Syndrome of hepatic cirrhosis, dystonia, polycythemia, and hypermanganesemia caused by mutations in SLC30A10, a manganese transporter in man. *Am. J. Hum. Genet.* **90,** 457–466 CrossRef Medline
17. Tuschl, K., Mills, P. B., Parsons, H., Malone, M., Fowler, D., Bitner-Glindzicz, M., and Clayton, P. T. (2008) Hepatic cirrhosis, dystonia, polycythaemia and hypermanganesaemia—a new metabolic disorder. *J. Inherit. Metab. Dis.* **31,** 151–163 CrossRef Medline
18. Wahlberg, K., Kippler, M., Alhamdow, A., Rahman, S. M., Smith, D. R., Vahter, M., Lucchini, R. G., and Broberg, K. (2016) Common polymorphisms in the solute carrier SLC30A10 are associated with blood manganese and neurological function. *Toxicol. Sci.* **149,** 473–483 CrossRef Medline
19. Leyva-Illades, D., Chen, P., Zogzas, C. E., Hutchens, S., Mercado, J. M., Swaim, C. D., Morrisett, R. A., Bowman, A. B., Aschner, M., and Mukhopadhyay, S. (2014) SLC30A10 is a cell surface-localized manganese efflux transporter, and parkinsonism-causing mutations block its intracellular trafficking and efflux activity. *J. Neurosci.* **34,** 14079–14095 CrossRef Medline
20. Mukhopadhyay, S. (2018) Familial manganese-induced neurotoxicity due to mutations in SLC30A10 or SLC39A14. *Neurotoxicology* **64,** 278–283 CrossRef Medline
21. Zogzas, C. E., Aschner, M., and Mukhopadhyay, S. (2016) Structural elements in the transmembrane and cytoplasmic domains of the metal transporter SLC30A10 are required for its manganese efflux activity. *J. Biol. Chem.* **291,** 15940–15957 CrossRef Medline
22. Hutchens, S., Liu, C., Jursa, T., Shawlot, W., Chaffee, B. K., Yin, W., Gore, A. C., Aschner, M., Smith, D. R., and Mukhopadhyay, S. (2017) Deficiency in the manganese efflux transporter SLC30A10 induces severe hypothyroidism in mice. *J. Biol. Chem.* **292,** 9760–9773 CrossRef Medline
23. Liu, C., Hutchens, S., Jursa, T., Shawlot, W., Polishchuk, E. V., Polishchuk, R. S., Dray, B. K., Gore, A. C., Aschner, M., Smith, D. R., and Mukhopadhyay, S. (2017) Hypothyroidism induced by loss of the manganese efflux transporter SLC30A10 may be explained by reduced thyroxine production. *J. Biol. Chem.* **292,** 16605–16615 CrossRef Medline
24. Chen, P., Bowman, A. B., Mukhopadhyay, S., and Aschner, M. (2015) SLC30A10: a novel manganese transporter. *Worm* **4,** e1042648 CrossRef Medline
25. Nishito, Y., Tsuji, N., Fujishiro, H., Takeda, T. A., Yamazaki, T., Teranishi, F., Okazaki, F., Matsunaga, A., Tuschl, K., Rao, R., Kono, S., Miyajima, H., Narita, H., Himeno, S., and Kambe, T. (2016) Direct comparison of manganese detoxification/efflux proteins and molecular characterization of ZnT10 protein as a manganese transporter. *J. Biol. Chem.* **291,** 14773–14787 CrossRef Medline
26. Zogzas, C. E., and Mukhopadhyay, S. (2018) Putative metal binding site in the transmembrane domain of the manganese transporter SLC30A10 is different from that of related zinc transporters. *Metallomics* **10,** 1053–1064 CrossRef Medline
27. Tronche, F., Kellendonk, C., Kretz, O., Gass, P., Anlag, K., Orban, P. C., Bock, R., Klein, R., and Schütz, G. (1999) Disruption of the glucocorticoid receptor gene in the nervous system results in reduced anxiety. *Nat. Genet.* **23,** 99–103 CrossRef Medline
28. Giusti, S. A., Vercelli, C. A., Vogl, A. M., Kolarz, A. W., Pino, N. S., Deussing, J. M., and Refojo, D. (2014) Behavioral phenotyping of Nestin-Cre mice: implications for genetic mouse models of psychiatric disorders. *J. Psychiatr. Res.* **55,** 87–95 CrossRef Medline
29. Postic, C., Shiota, M., Niswender, K. D., Jetton, T. L., Chen, Y., Moates, J. M., Shelton, K. D., Lindner, J., Cherrington, A. D., and Magnuson, M. A. (1999) Dual roles for glucokinase in glucose homeostasis as determined by liver and pancreatic beta cell-specific gene knock-outs using Cre recombinase. *J. Biol. Chem.* **274,** 305–315 CrossRef Medline
30. Ferruzza, S., Rossi, C., Scarino, M. L., and Sambuy, Y. (2012) A protocol for differentiation of human intestinal Caco-2 cells in asymmetric serum-containing medium. *Toxicol. In Vitro* **26,** 1252–1255 CrossRef Medline
31. Zorn, A. M., and Wells, J. M. (2009) Vertebrate endoderm development and organ formation. *Annu. Rev. Cell Dev. Biol.* **25,** 221–251 CrossRef Medline
32. Lee, C. S., Sund, N. J., Behr, R., Herrera, P. L., and Kaestner, K. H. (2005) Foxa2 is required for the differentiation of pancreatic α-cells. *Dev. Biol.* **278,** 484–495 CrossRef Medline
33. Garrison, W. D., Battle, M. A., Yang, C., Kaestner, K. H., Sladek, F. M., and Duncan, S. A. (2006) Hepatocyte nuclear factor 4α is essential for embryonic development of the mouse colon. *Gastroenterology* **130,** 1207–1220 Medline

34. Magnuson, M. A., and Osipovich, A. B. (2013) Pancreas-specific Cre driver lines and considerations for their prudent use. *Cell Metab.* **18,** 9–20 CrossRef Medline
35. Madison, B. B., Dunbar, L., Qiao, X. T., Braunstein, K., Braunstein, E., and Gumucio, D. L. (2002) Cis elements of the villin gene control expression in restricted domains of the vertical (crypt) and horizontal (duodenum, cecum) axes of the intestine. *J. Biol. Chem.* **277,** 33275–33283 CrossRef Medline
36. Jursa, T., and Smith, D. R. (2009) Ceruloplasmin alters the tissue disposition and neurotoxicity of manganese, but not its loading onto transferrin. *Toxicol. Sci.* **107,** 182–193 CrossRef Medline
37. Ma, R. E., Ward, E. J., Yeh, C. L., Snyder, S., Long, Z., Gokalp Yavuz, F., Zauber, S. E., and Dydak, U. (2018) Thalamic GABA levels and occupational manganese neurotoxicity: association with exposure levels and brain MRI. *Neurotoxicology* **64,** 30–42 CrossRef Medline
38. Bowman, A. B., and Aschner, M. (2014) Considerations on manganese (Mn) treatments for *in vitro* studies. *Neurotoxicology* **41,** 141–142 CrossRef Medline
39. Tuschl, K., Meyer, E., Valdivia, L. E., Zhao, N., Dadswell, C., Abdul-Sada, A., Hung, C. Y., Simpson, M. A., Chong, W. K., Jacques, T. S., Woltjer, R. L., Eaton, S., Gregory, A., Sanford, L., Kara, E., *et al.* (2016) Mutations in SLC39A14 disrupt manganese homeostasis and cause childhood-onset parkinsonism-dystonia. *Nat. Commun.* **7,** 11601 CrossRef Medline
40. Aydemir, T. B., Kim, M. H., Kim, J., Colon-Perez, L. M., Banan, G., Mareci, T. H., Febo, M., and Cousins, R. J. (2017) Metal transporter Zip14 (Slc39a14) deletion in mice increases manganese deposition and produces neurotoxic signatures and diminished motor activity. *J. Neurosci.* **37,** 5996–6006 CrossRef Medline
41. Jenkitkasemwong, S., Akinyode, A., Paulus, E., Weiskirchen, R., Hojyo, S., Fukada, T., Giraldo, G., Schrier, J., Garcia, A., Janus, C., Giasson, B., and Knutson, M. D. (2018) SLC39A14 deficiency alters manganese homeostasis and excretion resulting in brain manganese accumulation and motor deficits in mice. *Proc. Natl. Acad. Sci. U.S.A.* **115,** E1769–E1778 CrossRef Medline
42. Xin, Y., Gao, H., Wang, J., Qiang, Y., Imam, M. U., Li, Y., Wang, J., Zhang, R., Zhang, H., Yu, Y., Wang, H., Luo, H., Shi, C., Xu, Y., Hojyo, S., *et al.* (2017) Manganese transporter Slc39a14 deficiency revealed its key role in maintaining manganese homeostasis in mice. *Cell Discov.* **3,** 17025 CrossRef Medline
43. Nam, H., Wang, C. Y., Zhang, L., Zhang, W., Hojyo, S., Fukada, T., and Knutson, M. D. (2013) ZIP14 and DMT1 in the liver, pancreas, and heart are differentially regulated by iron deficiency and overload: implications for tissue iron uptake in iron-related disorders. *Haematologica* **98,** 1049–1057 CrossRef Medline
44. Guthrie, G. J., Aydemir, T. B., Troche, C., Martin, A. B., Chang, S. M., and Cousins, R. J. (2015) Influence of ZIP14 (slc39A14) on intestinal zinc processing and barrier function. *Am. J. Physiol. Gastrointest. Liver Physiol.* **308,** G171–G178 CrossRef Medline
45. Bouabid, S., Delaville, C., De Deurwaerdère, P., Lakhdar-Ghazal, N., and Benazzouz, A. (2014) Manganese-induced atypical parkinsonism is associated with altered basal ganglia activity and changes in tissue levels of monoamines in the rat. *PLoS One* **9,** e98952 CrossRef Medline
46. Liu, X., Sullivan, K. A., Madl, J. E., Legare, M., and Tjalkens, R. B. (2006) Manganese-induced neurotoxicity: the role of astroglial-derived nitric oxide in striatal interneuron degeneration. *Toxicol. Sci.* **91,** 521–531 CrossRef Medline
47. Cordova, F. M., Aguiar, A. S., Jr., Peres, T. V., Lopes, M. W., Gonçalves, F. M., Remor, A. P., Lopes, S. C., Pilati, C., Latini, A. S., Prediger, R. D., Erikson, K. M., Aschner, M., and Leal, R. B. (2012) *In vivo* manganese exposure modulates Erk, Akt and Darpp-32 in the striatum of developing rats, and impairs their motor function. *PLoS One* **7,** e33057 CrossRef Medline
48. Nam, J., and Kim, K. (2008) Abnormal motor function and the expression of striatal dopamine D2 receptors in manganese-treated mice. *Biol. Pharm. Bull.* **31,** 1894–1897 CrossRef Medline
49. Beaudin, S. A., Nisam, S., and Smith, D. R. (2013) Early life versus lifelong oral manganese exposure differently impairs skilled forelimb performance in adult rats. *Neurotoxicol. Teratol.* **38,** 36–45 CrossRef Medline
50. Beaudin, S. A., Strupp, B. J., Strawderman, M., and Smith, D. R. (2017) Early postnatal manganese exposure causes lasting impairment of selective and focused attention and arousal regulation in adult rats. *Environ. Health Perspect.* **125,** 230–237 CrossRef Medline
51. Hojyo, S., Fukada, T., Shimoda, S., Ohashi, W., Bin, B. H., Koseki, H., and Hirano, T. (2011) The zinc transporter SLC39A14/ZIP14 controls G-protein coupled receptor-mediated signaling required for systemic growth. *PLoS One* **6,** e18059 CrossRef Medline
52. Võikar, V., Kõks, S., Vasar, E., and Rauvala, H. (2001) Strain and gender differences in the behavior of mouse lines commonly used in transgenic studies. *Physiol. Behav.* **72,** 271–281 CrossRef Medline
53. Takeo, T., and Nakagata, N. (2011) Reduced glutathione enhances fertility of frozen/thawed C57BL/6 mouse sperm after exposure to methyl-β-cyclodextrin. *Biol. Reprod.* **85,** 1066–1072 CrossRef Medline
54. Livak, K. J., and Schmittgen, T. D. (2001) Analysis of relative gene expression data using real-time quantitative PCR and the $2(-\Delta\Delta C(T))$ method. *Methods* **25,** 402–408 CrossRef Medline
55. Selyunin, A. S., Iles, L. R., Bartholomeusz, G., and Mukhopadhyay, S. (2017) Genome-wide siRNA screen identifies UNC50 as a regulator of Shiga toxin 2 trafficking. *J. Cell Biol.* **216,** 3249–3262 CrossRef Medline
56. Selyunin, A. S., and Mukhopadhyay, S. (2015) A conserved structural motif mediates retrograde trafficking of Shiga toxin types 1 and 2. *Traffic* **16,** 1270–1287 CrossRef Medline

SLC30A10 transporter in the digestive system regulates brain manganese under basal conditions while brain SLC30A10 protects against neurotoxicity

Cherish A. Taylor, Steven Hutchens, Chunyi Liu, Thomas Jursa, William Shawlot, Michael Aschner, Donald R. Smith and Somshuvra Mukhopadhyay

J. Biol. Chem. 2019, 294:1860-1876.
doi: 10.1074/jbc.RA118.005628 originally published online December 17, 2018